This is the accepted manuscript of the article, which has been published in Sensors and Actuators B: Chemical. 2017, 239, 515-525. http://dx.doi.org/10.1016/j.snb.2016.08.040

Synergistic enhancement via plasmonic nanoplate-bacteria-nanorod supercrystals for highly efficient SERS sensing of food-borne bacteria

WeiQiang Wang[‡a], Ville Hynninen[‡b], Li Qiu[‡c], AiWen Zhang[c], Tibebe Lemma[d], NanNan Zhang[a], HongHua Ge[*a], J. Jussi Toppari[*d], Vesa P. Hytönen[b] and Jin Wang[*a]

[a] *Institute of Health Sciences and School of Life Science, AnHui University, Hefei, Anhui 230601, P.R. China*

[b] *BioMediTech, University of Tampere, FI-33520 Tampere, Finland and Fimlab Laboratories, FI-35520, Tampere, Finland*

[c] *Institute of Intelligent Machines, Chinese Academy of Sciences, Hefei, Anhui 230031, P. R. China*

[d] *University of Jyväskylä, Department of Physics, Nanoscience Center, P.O. Box 35, FI-40014, University of Jyväskylä, Finland*

KEYWORDS: Assembly, Asymmetric nanoparticles, Bacteria, SERS, Chemometrics

ABSTRACT

Bio-sensing techniques utilizing metallic nanoparticles as a probe have gained more and more attention and play today an important role in the detection of bacteria. To date, although several sensing materials have been tested, there is still a long way to go to achieve a fast, low-cost, ultrahigh sensitive and multifunctional substrate suitable for a universal biosensor for detection of bacterial cells. Here, we report a novel probe design based on anisotropic plasmonic nanoparticles organized to a biocompatible 3D bio-inorganic scaffold, i.e., nanoplate-bacteria-nanorod supercrystals (NBNS) with extremely high surface-enhanced Raman spectroscopic (SERS) activity as a model of synergistic plasmonic enhancement from nanoparticles and assembly. This unique structure of nanoparticles incorporated into supercrystal assembly allows efficient detection, identification and classification of cells and bacteria. In this design, the NBNS ensures that the target cells take advantage of the superior multifold increase in Raman scattering signals (electromagnetic enhancement from both types of nanoparticles), due to the geometry of the 3D scaffold. The excellent reproducibility and stability of NBNS substrates were confirmed by comparing the SERS activities of different substrates and analytes. Principal component analysis (PCA) applied to the SERS spectra clearly discriminated the homogeneous bacterial samples and their mixtures. Successful detection and identification of bacteria in model samples consisting of two representative bacteria blends in Fanta soft-drink were demonstrated via plasmonic bio-inorganic scaffold combined with PCA analysis. We believe that this work will greatly facilitate the development of ultrasensitive SERS probes for highly advanced biosensor, pioneering the use of SERS for controlling food safety.

1. Introduction

Food-borne bacteria, *e.g.*, *Escherichia coli*, *Salmonella etc*., have received more attention recently because of the low infectious dose and high health risk associated with these pathogens responsible for many food-borne diseases. Therefore, developing rapid, sensitive and reliable methods for assaying of food-borne pathogens are of an urgent demand. Many modern techniques, *e.g.*, microfluidic device [1,2], colorimetric [3,4], electrical device [5,6], fluorescence [7], microcantilever [8], electrochemical [9], chemiluminescence [10],.have been already used for detection of food-borne pathogens. Assembled nanoparticles have also been extensively studied due to their potential applications in electronic and optical sensors owing to their favorable photo-physics and spectroscopic properties. For instance, Chang *et al.* employed ultrasonic-assisted self-assembling of monolayer graphene oxide to fabricate a highly sensitive and selective field-effect transistor (FET) sensor for an assay of *Escherichia coli* bacteria [11]. Ondera *et al.* assembled gold nanopopcorns on single–walled carbon nanotubes as a hybridized sensor for rapid detection of *E. coli* bacteria [12].

As compared to other spectroscopic techniques, surface enhanced Raman scattering (SERS) based on plasmonic nanoparticles is a highly attractive method for detection of bacteria due to its high-sensitivity, reliability and reproducibility [12-16]. For example Wu *et al*. successfully utilized a silver nanorod array to obtain SERS signal of foodborne pathogenic bacteria in mung bean sprout samples by using a portable and handheld Raman system [17]. Particularly promising among possible designs for exploiting the unique optical properties of metallic nanoparticles on the functionality of sensing selective materials is the layer-by-layer (LBL) assembly protocol for fabrication of metamolecules. These strongly coupled plasmonic

assemblies as metamaterials have been extensively investigated because of their inherent highly-sensitive SERS properties originating from the densely packed “hot-spots” within the nanoassembly [17-22].

In this paper, we utilize plasmonic nanoplates and nanorods supercrystal to develop a novel highly sensitive SERS protocol. It is based on 3D bio-inorganic supercrystal assembly of anisotropic nanoparticles of various types, i.e., nanoplate-bacteria-nanorod supercrystals (NBNS), and used here for label-free assay of different Gram-positive and Gram-negative bacteria. The novel construction of NBNS ensures that the target cells take an advantage of the superior multifold enhanced Raman scattering enabling discrimination of different bacteria species based on their SERS spectra. Furthermore, to demonstrate the applicability of the method especially within the area of the food industry, we recorded SERS spectra from bacteria embedded in soft-drink and obtained a clear separation of them from the surrounding matrix with high correlation by using principal component analysis (PCA). This statistical technique coupled with the high sensitivity of the SERS data opens the door to the applicability of this biosensing platform to food quality control.

2. MATERIALS AND METHODS

2.1 Materials

$HAuCl_4 \cdot 4H_2O$ (99.9%), $NaBH_4$ (99%), Vitamin C (99.9%), cetyltrimethylammonium bromide (CTAB) (99%), $AgNO_3$ (99.9%), 2-Quinolinethiol (2-QT), poly(sodium styrenesulphonate) (PSS), trisodium citrate and vancomycin hydrochloride were purchased from Sigma-Aldrich, Gram-negative *Salmonella enterica* (*S. enterica*) bacteria (ATCC 14028), Gram-

negative *Escherichia coli* (*E. coli*) (CMCC 44568), Gram-positive *Staphylococcus xylosus* (*S. xylosus*) (ZSL-3) were purchased from China General Microbiological Culture Collection Center (CGMCC). The deionized water that was used throughout the experiments was purified by using a Milli-Q system.

2.2 Fabrication of plasmonic 3D nanorod supercrystals

All of the silicon chips with (1x1 cm^2) were firstly cleaned by ultrasonication in acetone, ethanol and MilliQ water for 1h. Then, the silicon chips were immersed into a piranha solution (H_2SO_4:H_2O_2 = 3:1) at 80˚C for 1 h and rinsed with Milli-Q water. The clean silicon chips were dried by nitrogen gas flow at room temperature.

Synthesis of nanorods is explained in supporting information (S1.1). Two samples of 1 mL as-prepared nanorod solution was centrifuged at the 8000 rpm for 10 min to remove the excess CTAB surfactants and the precipitates were redispersed in 50 μL and 200 μL Milli-Q solution, respectively. Then, two samples of the obtained nanorod colloidal solution with 5 μL were dropped on the cleaned silicon substrate and the chips were kept in Petri dish under cover at humid environment with temperature 20°C for 24 h so as to yield vertical and parallel 3D nanorod supercrystals, respectively.

2.3 Bacterial culturing

Lyophilized powder of *E. coli* bacteria (CMCC44568), *Salmonella enterica* (*S. enterica*) (ATCC 14028) and *Staphylococcus xylosus* (*S. xylosus*) bacteria (ZSL-3) were resuspended to 5mL LB nutrient and cultivated for 14h in shaking incubator (200 rpm), respectively. Bacterial

suspension was plated on an LB agar plate using sterile plastic inoculating loops to carry out plate streaking and the plate was settled in a constant temperature incubator and cultivated for 14h to obtain single colonies. Single colonies were collected via sterile plastic inoculating loops and dissolved into 1 mL aquae sterilisata. 100 μL bacteria solution was coated on LB agar base and incubated in constant temperature incubator at 37 °C. Subsequently, the bacteria was dispersed in Milli-Q water and centrifuged for 10 min at 3000 rpm so as to protect the cell membrane. Finally, the supernatant liquid was discarded and the bacterial cells were redispersed in Milli-Q water. The purified bacteria were diluted to a concentration of 10^3 cfu/mL. The density of bacteria cells was determined by counting the number of colonies grown on the Petri dish after 12 h of cultivation.

2.4 Fabrication of 3D scaffold of plasmonic nanoplate aggregate-bacteria-nanorod supercrystals

The plasmonic 3D vertical nanorod supercrystal substrate was immersed into 10^{-2} M aqueous solution of vancomycin hydrochloride for 1 h and then dried in air to yield a vancomycin-coated supercrystal substrate. 1 mL of the bacterial suspension was placed on the as-prepared supercrystal substrate and then settled in a constant temperature incubator for 1 h at 37°C. After that, the substrate was washed three times by using Milli-Q water. The bacteria-immobilized supercrystal substrate was immersed into freshly prepared Ag nanoplates to obtain the 3D scaffold of plasmonic nanoplate aggregate-bacteria-nanorod supercrystal and then dried in air for characterization and measurement. Synthesis of Ag nanoplates is shown in supporting information (S1.2).

2.5 Characterization

Scanning electron microscope (SEM) images were acquired with a Quanta200FEG. UV-Vis-NIR absorption spectra were recorded by using a Solidspec-3700 spectrophotometer. SERS experiment were performed via Renishaw Invia Reflex Raman spectrometer equipped with a 280 mW semiconductor laser emitting at a 785 nm line. Surface enhanced Raman spectra were collected through 100 x objective lens at the condition of 8.5 mW laser power and10 s integration time.

2.6 Chemometrics

The Unscrambler® X software (version 10.3, CAMO Software; Oslo, Norway) including Unscrambler Service Pack 2014 was used to analyze SERS spectra. First, the spectra were visually inspected and significantly differing spectra were removed from the analysis. Then, linear baseline correction with baseline offset and standard normal variate (SNV) were used as a pretreatment. 400.78 cm^{-1} and 1761.03 cm^{-1} wavenumbers were used as the defining wavelengths in the linear baseline correction. In the baseline offset the lowest point in the spectrum is subtracted from all the variables (wavenumbers) and, thus, the minimum value is set to 0 and the rest of the variables have positive values. Following the baseline correction, the spectra were normalized using the standard normal variate (SNV) technique, which is a commonly used mathematical transformation method to remove multiplicative scatter and particle-size interferences from spectral data [23, 24]. Following the pretreatments, mean centered principal component analysis (PCA) was performed in the 400 cm^{-1} to 1800 cm^{-1} range. Initially, the 800 cm^{-1} to 1800 cm^{-1} range was also tested but the longer range produced more accurate results. Thus, the 400 cm^{-1} to 1800 cm^{-1} range was used throughout the experiments.

PCA reduces the dimensionality of the data set while retaining the dominant features that contribute most to its variance. This allows categorization of the data according to spectral features that might otherwise be hardly distinguishable [25, 26].

3. RESULTS AND DISCUSSION

As shown in Fig. 1, the assembling protocol of the NBNS can be described as three steps: (I) fabricating 3D plasmonic nanorod supercrystal on a chip; (II) immobilization of bacteria on the plasmonic supercrystal; (III) deposition of plasmonic nanoplates on the bacteria. This layer-by-layer fabricated hybridized superstructure substrate has several advantages: (I) 3D nanorod supercrystal provides a large-scaled uniform substrate; (II) bacteria immobilized on the vancomycin coated supercrystal provides a robust scaffold for aggregating nanoplates; (III) synergistic plasmonic enhancement from the 3D hybridized nanoplate aggregates and the nanorod supercrystal.

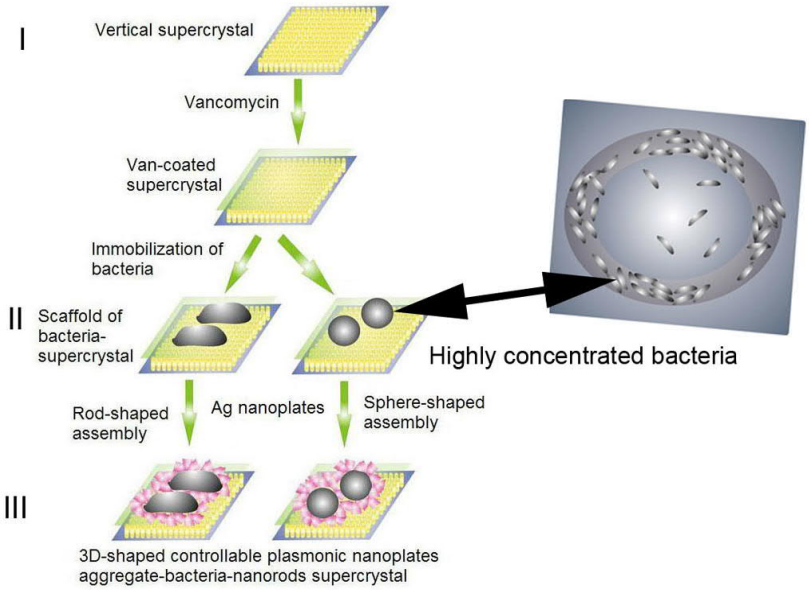

Fig. 1. Cartoon graph of the protocol of fabricating the 3D-shaped controllable plasmonic nanoplate aggregate-bacteria-nanorod supercrystal and utilizing it for label-free sensing of bacteria.

3.1. Fabrication of 3D plasmonic nanorod supercrystal.

As an initial step for the layer-by-layer (LBL) fabrication of NBNS, Au nanorods with a longitudinal localized surface plasmon resonance (LSPR) at 783 nm (shown in Fig. S1) were produced (see supporting information for details). The excellent overlap of the LSPR band with the utilized excitation laser line at 785 nm yields optimized plasmonic enhancement. Thanks to the stronger LSPR effects of nanosilver components as compared to nanogold, it is necessary to give a Ag shell coating on the Au nanorods. As shown in Fig. S1, the sensitive longitudinal LSPR band can be remarkably blueshifted in contrast to the insensitive transverse LSPR band, around 500 nm, which only slightly blueshifts when Au nanorod is coated with Ag shell. The more silver is deposited the more the LSPR bands are shifted as clearly seen from Fig. S1. Additionally, in the sample with the highest amount of Ag, a broad LSPR band located around 400 nm, indicating formation of Ag components in addition to the Au/Ag core-shell nanorods. Herein, Au nanorods with the thinnest Ag shell, corresponding to the longitudinal LSPR band blueshifted from 783 nm to 765 nm, were selected as a building blocks for the 3D supercrystal, providing maximum plasmonic coupling with the excitation line of 785 nm. As reported from previous study, the plasmonic band of core-shell nanorod supercrystal is dramatically brodened and enranged from Visible to NIR regions as compared to that of core-shell nanorods colloid solution, which can be efficently coupling with different exciation laser lines [27].

3D supercrystal of the Au/Ag core-shell nanorods described above was formed on a piranha-treated silicon chip by a controllable slow-evaporation method. In contrast to what is observed

for nanospheres, it is difficult for ellipsoids to yield a 3D supercrystal surrounding coffee-ring on a chip, which is ascribed to a stronger interparticle attraction between the anisometric particles [28]. However, surfactant coating of the ellipsoids can be used to change the assembling process on a chip. For example, mediation of a surfactant CTAB is an important effect for assembly of nanorods to form supercrystal because it can inhibit interfacial deformation. As a result, tension of the liquid drop is decreased so as to recover the coffee-ring effect. Although the coulombic repulsion from positive charges of CTAB coating can lead to a dispersion of nanorods, micelle molecule CTAB as a depletant should drive entropic stacking of the nanorods. Thus, the 3D nanorod supercrystal can be efficiently fabricated on the basis of the balance of the depletion attraction, attractive van der Waals interaction and the repulsive force. Depending on the concentration of nanorods, two kinds of supercrystals can be formed on a chip, *i.e.*, supercrystals with the vertical or parallel alignment of the nanorods. As seen from Fig. S2, stacking of the high-density nanorods and low-density nanorods can yield 3D vertical and parallel supercrystals, respectively, along the coffee-ring line on a chip via slow-evaporation approach. In contrast to the 3D parallel nanorod supercrystal, the vertical nanorod supercrystal is obviously more robust as a number of incoming nanorods can be effectively supported by adjacent standing nanorods so as to form supercrystal with uniform alignment direction.

We compared the two kinds of supercrystal substrates for binding of bacteria in order to find out the feasibility of them for the investigation of bacteria. As shown in Fig. S3, the large-scale uniform orientation of parallel nanorod supercrystal has been changed to a short-ranged order after the binding of bacteria. In contrast, the long-range order of vertical nanorods supercrystal (shown in Fig. 2A-C) can be effectively retained so as to form a dot-like dispersion. This implies

that vertically aligned nanorod supercrystal is robust enough to be utilized as an excellent substrate for sensing of bacteria in contrast to the parallel nanorod supercrystal.

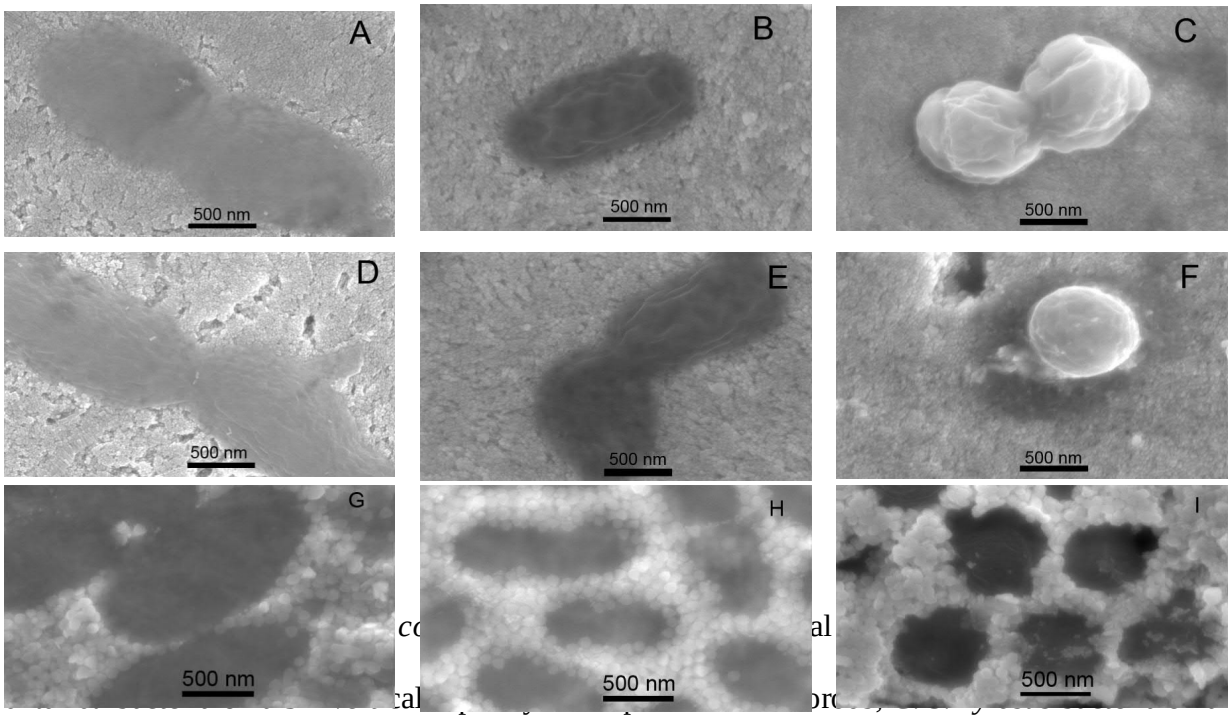

3D vertical supercrystal of plasmonic nanorods; D: *E. coli* on a vancomycin-coated 3D vertical supercrystal of plasmonic nanorods; E: *S. enterica* on a vancomycin-coated 3D vertical supercrystal of plasmonic nanorods; F: *S. xylosus* bacteria on a vancomycin-coated 3D vertical supercrystal of plasmonic nanorods; G: plasmonic 3D nanoplate aggregate-*E. coli*-vertical nanorod supercrystal; H: plasmonic 3D nanoplate aggregate-*S. enterica*-vertical nanorod supercrystal; I: plasmonic 3D nanoplates aggregate-*S. xylosus*-vertical nanorod supercrystal.

3.2. SERS properties of the 3D plasmonic nanorod supercrystal.

To evaluate SERS properties of the two different supercrystals, we utilized 2-quinolinethiol (2-QT) as a Raman probe due to its large Raman scattering cross section and attached it to a vertical and a parallel nanorod supercrystal. Fig. S4 shows the SERS spectra of self-assembled 2-QT over the supercrystal substrates. According to random point-to-point SERS analysis, the

SERS enhancement factor of the vertical nanorod supercrystal is clearly higher than that observed with the parallel nanorod supercrystal (shown in Fig. S4). Also, from the analysis of the intense band at 1373 cm^{-1} assigned as an aromatic ring stretching, relative standard deviation (RSD) of the Raman signal intensity can be calculated based on the 30 random points. According to the point-to-point analysis of the substrate, variation in the SERS signal at 1373 cm^{-1} measured for the vertical 3D nanorod supercrystal (RSD = 5.57%) is lower than that measured for the parallel supercrystal (8.42%) (Fig. S5). To further test the homogeneity of the signal intensity of vertical 3D nanorod supercrystal, SERS mapping was performed over an area (10μm x 10μm, step size of 2μm) (shown in Fig. 3). In all, 30 Raman spectra were collected for each map.

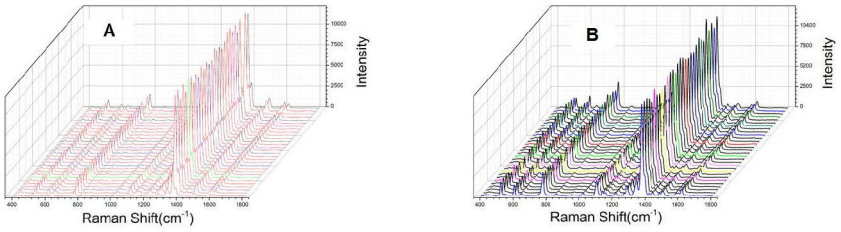

Fig. 3. Raman Spectra of SERS mapping in two different regions (10μm x 10μm, step size of 2μm) obtained from vertical 3D nanorod supercrystal.

As a result, variation in the SERS signal at 1373 cm^{-1} measured for the vertical 3D nanorod supercrystal (RSD = 4.29 % and RSD = 4.34% for each mapping) (shown in Fig. 4), indicating the homogeneity is good enough for practical application. Therefore, the reproducibility of the 3D vertical nanorod supercrystal is better than the 3D parallel nanorod supercrystal so as to be selected as a uniform and sensitive SERS substrate.

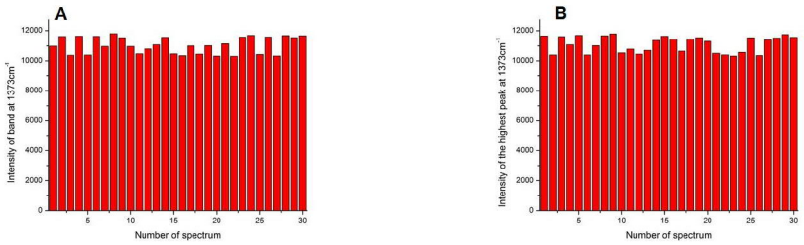

Fig.4. Variation of SERS intensity of 2-quinolinethiol (2-QT) by SERS mapping obtained from the two different regions of vertical 3D nanorod supercrystal.

3.3. Immobilization of bacteria on the plasmonic supercrystal.

Immobilization of bacteria on a 3D nanorod supercrystal can be enhanced by using antibiotics. Lv *et al*. explored a sensitive real-time electrochemical detection of disease related bacteria on the basis of a nanostructured Au electrode modified with indium tin oxide (ITO), through the antibiotics agent doxorubicin [29]. Chung *et al* demonstrated that antibiotics, *e.g*., vancomycin and daptomycin, can be used to immobilize gram-positive bacteria via their cell wall [30].

Vancomycin can easily form noncovalent asymmetric dimmers of vancomycin via multiple hydrogen bond, which is favorable to generate nanometer-sized vancomycin aggregates [31]. As reported previously, self-association of vancomycin monomers by aid of collective back-back and side-side interactions contributes to formation of large supramolecular complex [32]. Moreover, theoretical results suggest that variation in molecular conformation can be caused by the multiple hydrogen bond, which induces dramatically intramolecular mode coupling[32]. Therefore, although vancomycin coating layer can be directly contacted with nanorod supercrystal receiving much stronger electromagnetic enhancement effects compared to more rigid bacterial cell wall, their Raman spectral features have been dramatically submerged leading

to serious brodening (shown in Fig. S6) due to various configurations for vancomycin aggregating to nanoparticles.

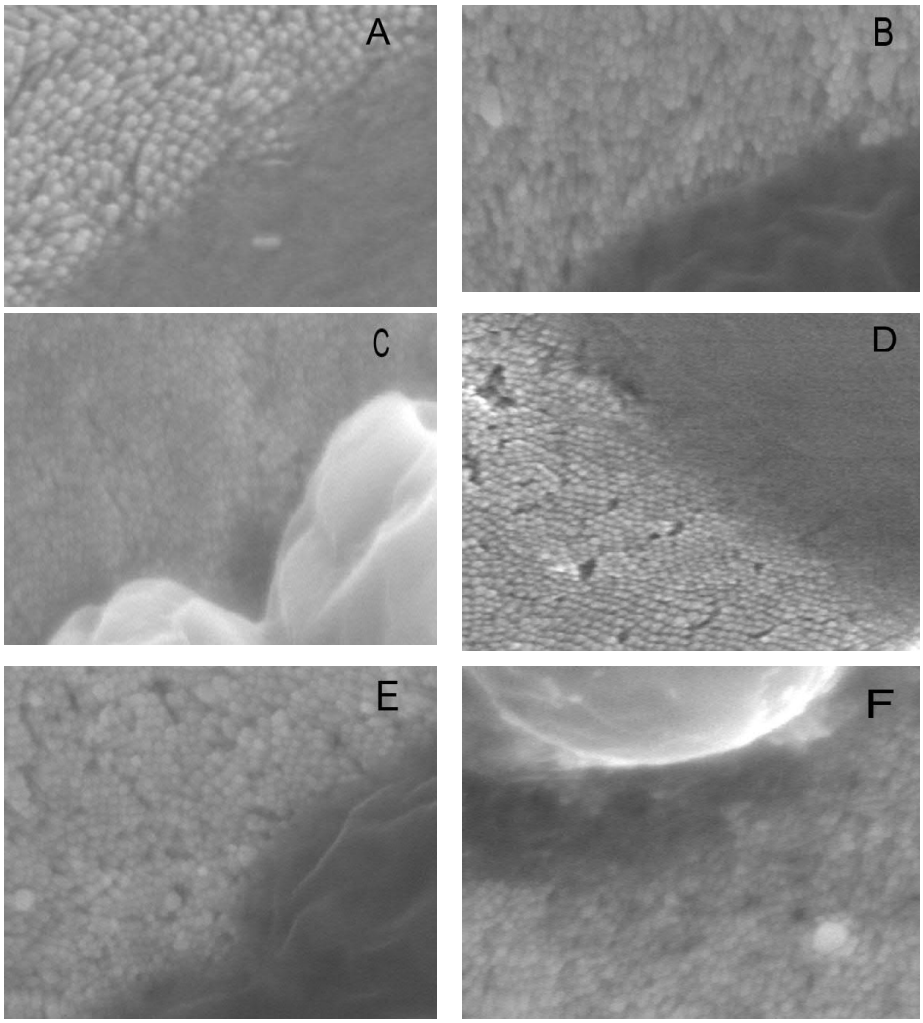

Fig. 5. Expansion of SEM images of A: *E. coli* on a 3D vertical supercrystal of plasmonic nanorods; B: *S. enterica* on a 3D vertical supercrystal of plasmonic nanorods; C: *S. xylosus* on a 3D vertical supercrystal of plasmonic nanorods; D: *E. coli* on a vancomycin-coated 3D vertical supercrystal of plasmonic nanorods; E: *S. enterica* on a vancomycin-coated 3D vertical

supercrystal of plasmonic nanorods; F: *S. xylosus* on a vancomycin-coated 3D vertical supercrystal of plasmonic nanorods

The 3D vertical nanorod supercrystal provides a round top-surface with nanometer-scale gaps ("nanogaps") as binding sites for vancomycin so as to trap vancomycin nanoparticles with a few nanometers in diameter. Moreover, the nanogaps between the adjacent nanorods can act as important hot-spots (plasmonic gap modes) for amplifying exponentially the Raman scattering. As shown in Fig. 5A-C, in the case of the 3D-vertical nanorod supercrystal without vancomycin, the cell wall of bacteria can only protrude onto round top-surface. In contrast, the cell wall of bacteria can penetrate into a vancomycin-coated 3D-vertical nanorod supercrystal due to the vancomycin nanoparticles entrapped within the nanogaps, as shown in Fig. 5D-F. Furthermore, a stretched shadow around the cell wall of bacteria can be clearly observed on the vancomycin-coated 3D supercrystal conversely to the bacteria on a 3D supercrystal without vancomycin. When a cell wall of bacteria is partially entrapped into hot-spot of a nanogap via vancomycin immobilization, great enhancement on a Raman signal of bacteria is expected. Indeed, as observed from Fig. 6, the intensity of the Raman signal of bacteria, *S. xylosus*, *S. enterica* and *E. coli* was increased *ca*. 9 times, 5 times and 3 times, respectively. The capturing ability of the vancomycin-coated 3D nanorod supercrystal is different for Gram+ and Gram- bacteria due to a different cell wall structure of Gram+ and Gram- bacteria, and is reflected in both SEM observations and SERS enhancement. Compared to Gram- bacteria, *e.g.*, *E. coli* and *S. enterica*, the interaction between vancomycin and peptidoglycan in the cell wall of Gram+ bacteria, *e.g.*, *S. xylosus*, is much stronger. This can be related to the fact that cell walls of *Staphylococcus* could be destroyed and a release of cytoplasmic components may happen thanks to vancomycin

attacking the cell wall of bacteria by aid of hydrogen bonding to N-acetylglucosamine/N-acetylmuramic acid-peptide linker, peptidoglycan and teichoic-acid, reflected from the more obvious rim attached to the substrate (shown in Fig. 5F).

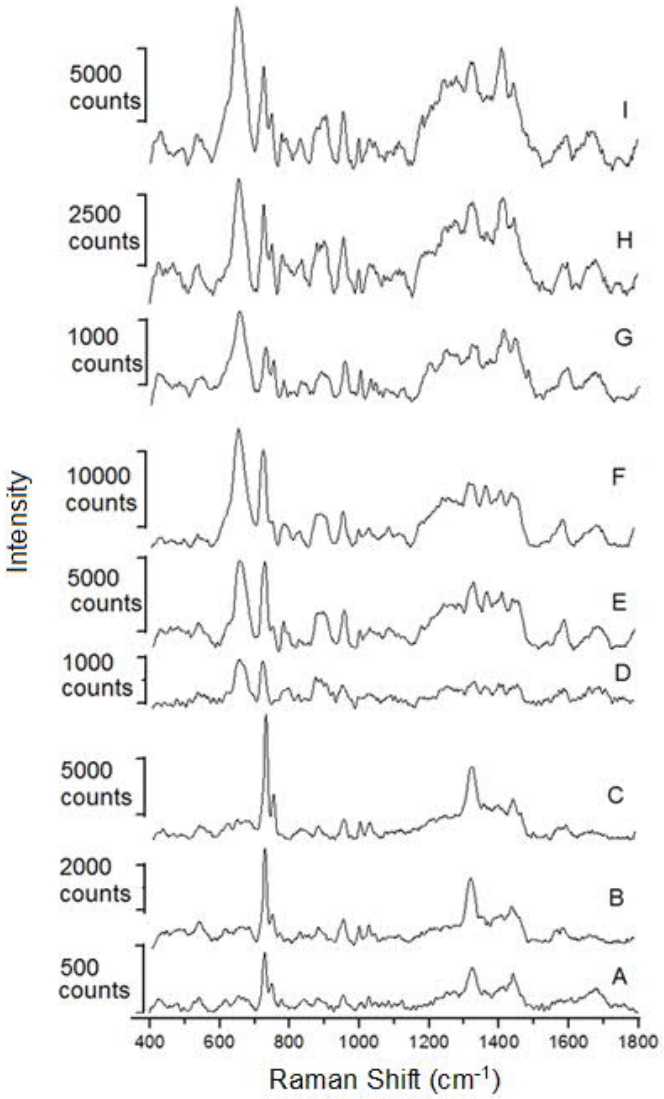

Fig. 6. SERS spectra of A: *S. xylosus* on a plasmonic vertical nanorod supercrystal, B: *S. xylosus* bacteria on a vancomycin-coated plasmonic vertical nanorod supercrystal, C: *S. xylosus* embedded in a plasmonic nanoplate aggregate/vertical nanorod supercrystal, D: *S. enterica* on a plasmonic vertical nanorod supercrystal, E: *S. enterica* on a vancomycin-coated plasmonic vertical nanorod supercrystal, F: *S. enterica* embedded in a plasmonic nanoplate

aggregate/vertical nanorod supercrystal, G: *E. coli* on a plasmonic vertical nanorod supercrystal, H: *E. coli* on a vancomycin-coated plasmonic vertical nanorod supercrystal, I: *E. coli* embedded in a plasmonic nanoplate aggregate/vertical nanorod supercrystal.

The absorption efficiency of bacteria in NBNS is depended on the vancomycin coated-nanorod supercrystal. The capturing ability of van-nanorod supercrystal has been found to be determined by the coverage of the vancomycin coating. In order to obtain the dependence of the adsorption efficiency about the coverage of vancomycin on the nanorod supercrystal, the ratio between the number of the staphylococcus bacteria immobilized on the supercrystal substrate with vancocymin and without vancomycin. Fig. S7 illustrates that the ratio increase accompany with increasing vancomycin coating coverage of van-nanorod supercrystal.

However, the dependence of the SERS ability of *S. xylosus* bacteria on the different van coveraged nanorod supercrystal can be reflected from Fig. S7 It should be pointed out that the ratio of Raman enhancement reaches the maximum and subsequent decrease with alteration of vancomycin converage on the NBNS substrate. The optimized coverage indicate that increasing the Raman signal of absorbed bacteria can be determined via increasing the vancomycin coverage, leading to more bacteria receiving SERS effects. However, the distance between bacteria and plasmonic supercrystal can be increased, which causes the loss of direct enhancement from the nanorod supercrystal.

3.4. Deposition of plasmonic nanoplates on the bacteria

Due to the height (*ca.* 100 nm~300 nm) of bacterial cells, *e.g.*, *E. coli* (Fig. S7), they protrude from the surface of the 3D vertical nanorod supercrystal. Therefore, only the interface between the lower edge of the bacteria and the endcap of the nanorod array can be effectively affected by a near-field plasmonic effects, implying that only Raman signal from the interface can be enhanced. Therefore, it is necessary to further deposit plasmonic nanoparticles into the gaps between the bacterial cells in order to embed the bacteria into the aggregates of plasmonic nanoparticles. In this case, the electron transfer between the plasmonic nanoparticle aggregates and nanorod supercrystal leads to additional strengthening of the plasmonic field. On the other hand, the bacteria can receive electromagnetic enhancement from the plasmonic field of 3D nanorods supercrystal at the bottom of the hybridized scaffold. Simultaneously, the bacteria can also obtain the electromagnetic enhancement from plasmonic field of the 3D nanoparticles aggregates amongst the gaps of hybridized scaffold.

Triangular silver nanoplate is a powerful candidate within anisotropic plasmonic nanoparticles for constructing the chemical or biological sensors due to their thinness as compared to nanosphere, leading to a significant extension of the electromagnetic field farther from their surface. Furthermore, the three tips of the nanoplates with larger refractive index sensitivity dramatically contributes to their near-field electromagnetic enhancement localized the tips [33-35]. As shown in Fig. S8A, the nanoplates with triangular tips can be clearly observed. By the present seed-mediated protocol (see supporting information for details), continuous tuning of LSPR band corresponding to the dipole resonance of Ag nanoplates, can be obtained ranging from visible region to near-infrared region (shown in Fig. S8B). We selected the Ag nanoplates with LSPR band located around 795 nm for the experiment as they produce maximum overlap

with the laser line excitation at 785 nm, which further leads to stronger SERS enhancement. Therefore, the selected Ag nanoplates were used to efficiently fill the gaps between the immobilized bacteria to form rodlike or spherical nanoaggregates.

Detailed comparison of averaged SERS spectra (shown in Fig. S9) of *S. xylosus* bacteria adhered on different combinations of the substrates, suggests that the enhancement from the combined 3D Ag nanoplate aggregate-nanorod supercrystal is clearly higher than those from the 3D nanorod supercrystal or Ag nanoplate aggregates alone, indicating that synergistic enhancement from both Ag nanoplates aggregates and nanorod supercrystal can maximize the Raman signal of bacteria.

3.5. Analysis of SERS spectra of Gram+ and Gram- bacteria in the NBNS

Based on the plasmonic 3D hybridized bio-inorganic scaffold, the inherent Raman vibrational signal of bacteria is dramatically amplified so that Raman signals of different bacteria can be clearly discriminated. Compared to Gram- bacteria, *e.g., S. enterica* and *E. coli*, SERS spectrum of Gram+ bacteria *S. xylosus* is simpler due to a relatively simple structure of the cell wall. Detailed assignment of vibrational bands of bacteria in SERS spectra have been given in Tabs S1-S3.

As observed from Fig. 6, the vibrational band between 600~800 cm^{-1} can be described as a fingerprint region of bacterial DNA/RNA due to the dominant SERS signal of adenine and guanine compared to the others. The order of the SERS cross-section is adenine > guanine > cytosine > thymine [36, 37]. Particularly, the bands at *ca.* 650 cm^{-1} and 730 cm^{-1} are clearly

different for all the three bacteria studied here. In the case of Gram+ bacteria, *e.g.*, *S. xylosus*, the band at 730 cm^{-1} is very strong in contrast to the very weak band at 666 cm^{-1}, suggesting that activity of the ring stretching of adenine is stronger than that of guanine. However, in the case of Gram- bacteria, *e.g.*, *S. enterica*, two strong vibrational bands at 653 cm^{-1} and 727 cm^{-1} indicate that activities of the ring stretching of adenine and guanine are both high. In contrast, in another representative Gram- bacteria, *e.g.*, *E. coli*, the band at 658 cm^{-1} assigned as guanine vibration is obviously stronger than the band at 730 cm^{-1} ascribed to adenine vibration.

Besides the fingerprint region between 600~800 cm^{-1}, another obviously discriminating region in the SERS spectra of bacteria is observed between 1100~1500 cm^{-1}. However, in contrast to Gram+ bacteria, the vibrational bands located at the region are quite complicated for Gram- bacteria due to multiple components in different bacteria. As far as *S. xylosus* is concerned, the two strong vibrational bands (1327 cm^{-1} and 1449 cm^{-1}), can be assigned as ring stretching of cytosine/uracil and C-H deformation, respectively. Although analogous vibrational bands of Gram- bacteria could be observed within the spectral region, the profile of the series of bands is different, *i.e.*, intensity ratios of the bands located at *ca.* 1329 cm^{-1}, 1370 cm^{-1}, 1413 cm^{-1} and 1454 cm^{-1}, can be acted as another fingerprint spectral region for discriminating bacteria. It should be pointed out that the weak C=O stretch located at *ca.* 1660 cm^{-1} originating from Amide I of protein, and C-N-H deformation located at *ca.* 1280 cm^{-1} originating from Amide III, can be observed for all three bacteria. However, the similarities of the profile and position of the vibrational band of the different bacteria make it difficult to use them as fingerprint bands.

In orde to obtain a limit of Detection (LOD) of Gram-negative bacteria *E. coli* and Gram-positive bacteria *S. xylosus* via NBNS SERS substrate, we plotted the SERS peak intensity of *E.*

coli at I_{658} and SERS peak intensity of *S. xylosus* at I_{730} against the bacterial concentration (Fig. S10-S11), respectively. As far as each concentration is concerned, mean and standard deviation of the peak intensities can be obtained on the basis of the collected 6 spectra from two different substrates. In the present case, the LOD of the SERS detection can be determined by the lowest concentration at which a obvious bacterial SERS spectrum can be obtained. As shown from Fig. S10B and S11B, the lowest concentration of *E.coli* and *S.xylosus* bacteria that can be detected is 10^3 CFU/mL and 10^2CFU/mL, respectively.

3.6. Analysis of SERS spectra of mixed bacteria solutions.

On the basis of SERS analysis of the three bacteria, experiments with mixtures of different bacteria with different ratios has been carried out to test multiplex sensing abilities via NBNS. As far as the SERS spectra of the two Gram- bacteria, *i.e.*, *E. coli* and *S. enterica* are concerned, the intensity ratio of bands at *ca*. 650 cm^{-1} and 730 cm^{-1} for the mixed bacteria (with ratio 1:1) is different from the pure bacteria as shown Fig. 7. In the case of *S. enterica*, the band at 650 cm^{-1} is obviously lower than the band at 730 cm^{-1}; on the contrary, as for *E. coli* bacteria, the band at 650 cm^{-1} is dramatically higher than that at 730 cm^{-1}. However, the intensities of the two bands in the mixed bacteria sample with ratio 1:1 are very close, implying that it is possible to discriminate between the mixture of bacteria and pure bacteria. When the ratio of *E. coli* and *S. enterica* is changed from 1:1 to 1:2, the intensity ratio of vibrational bands at 650 cm^{-1} and 730 cm^{-1} is remarkably decreased, implying that it is also possible to use this method to determine the concentration of the bacteria in a mixture. Furthermore, as the ratio of *E. coli* and *S. enterica* is continually increased to 1:5, the SERS spectra of mixed bacteria appears similar to the SERS

spectrum of *S. enterica*, which implies that the percentage of salmonella bacteria in the bacteria mixture is dominant.

Additionally, another fingerprint spectral region between 1100 cm^{-1} and 1500 cm^{-1}, can also be utilized to discriminate the mixed bacteria and pure bacteria. As seen from Fig. 7, the profiles of the bands of the mixed bacteria are quite different from the pure bacteria, *i.e.*, *S. enterica* and *E. coli*. It should be mentioned that the intensities of the bands assigned as C-O, C-C stretch, C-O-H deformation, located at the region of 900 cm^{-1} ~ 1200 cm^{-1}, in the SERS spectra are obviously increased as compared to the pure bacteria.

As far as the mixed Gram- and Gram+ bacteria are concerned (see Fig. S12), *E. coli* and *S. xylosus* were also mixed with ratios of 1:1, 1:2 and 1:5 to study the effects of kinds of bacteria and concentration on the SERS signal. As shown by Fig. S12, the SERS spectra of mixed *E. coli* and *S. xylosus* with ratio 1:1, is different from SERS spectra of pure *E. coli* and *S. xylosus* samples. As compared to the SERS spectra of pure *S. xylosus*, the band at 660 cm^{-1} can be clearly observed in the mixture, indicating the presence of *S. enterica* in the sample. On the other hand, the band at 1326 cm^{-1} in the SERS spectra of the mixture is remarkably stronger than the other vibrational bands located in the region from 1100 cm^{-1} to 1500 cm^{-1}.

Because in real samples the density of *E. Coli* is usually higher than that of either *S. enterica* or *S. xylosus*, we compare the SERS spectrum of *E. Coli* bacteria and *S. xylosus* bacteria with the ratio of 10:1 to the 1:1 mixture or monospecies. As shown from Fig. S13, the relative intensity ratio of the bands at 730 cm^{-1} and 658 cm^{-1}, can be dramatically changed accompany with the ratio changing from 1:1 to 10:1. For example, the intensity of the band at 658 cm^{-1} in the mixture with ratio 1:1, is much lower than that of the band at 730 cm^{-1}; however, the intensity of the band

at 658 cm^{-1} in the mixture with ratio 10:1 can be comparable to that of the band at 730 cm^{-1}, suggesting that the mixture can be differentiated from the mixture with ratio of 1:1. O the other hand, the relative intensity of the the band at the bands at 730 cm^{-1} and 658 cm^{-1} in the mixture with the ratio of 10:1 (shown in Fig. S13) appears somewhat different from the monospecies (E.Coli bacteria), which implies it is possible to discriminate extreme amounts of E-Coli bacteria in the mixture samples fom the monospecies.

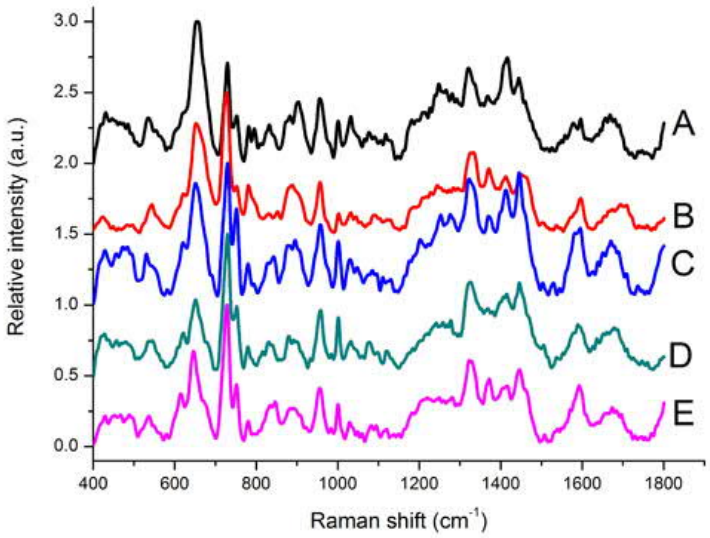

Fig. 7. A comparison on normalized SERS spectra of the mixed and monospecies bacteria collected from a 3D plasmonic nanoplate aggregate-bacteria-vertical nanorod supercrystal. A: Gram- *E. coli*; B: Gram- *S. enterica*; C: mixture of *E. coli* and *S. enterica* with ratio 1:1; D: mixture of *E. coli* and *S. enterica* with ratio 1:2; E: mixture of *E. coli* and *S. enterica* with ratio 1:5.

3.7. PCA analysis of monospecies and mixed- bacteria SERS spectra.

When utilizing principal component analysis (PCA) on monospecies samples and the mixtures (1:1 ratio) of two different bacterial species together, the monospecies samples formed their own distinct clusters, as shown in Fig. 8a. Thus, the ability of PCA to identify monospecies samples based on their SERS spectra appeared possible. The mixture clusters, in turn, were partially overlapping and located in between of the monospecies samples. However, this was expected, because the mixtures contain features from the two different species and, therefore, they inevitably share some common characteristics. Nonetheless, by evaluating enough PCs, also the identification of the mixtures was shown to be possible, as is demonstrated in Fig. 8b where the clusters are plotted according to PC1 and PC5. Cumulatively, the first five PCs explained 72 % of the total data variance. The SERS spectra of the monospecies samples and 1:1 mixed samples are shown in Supplementary Information Fig. S14~S19.

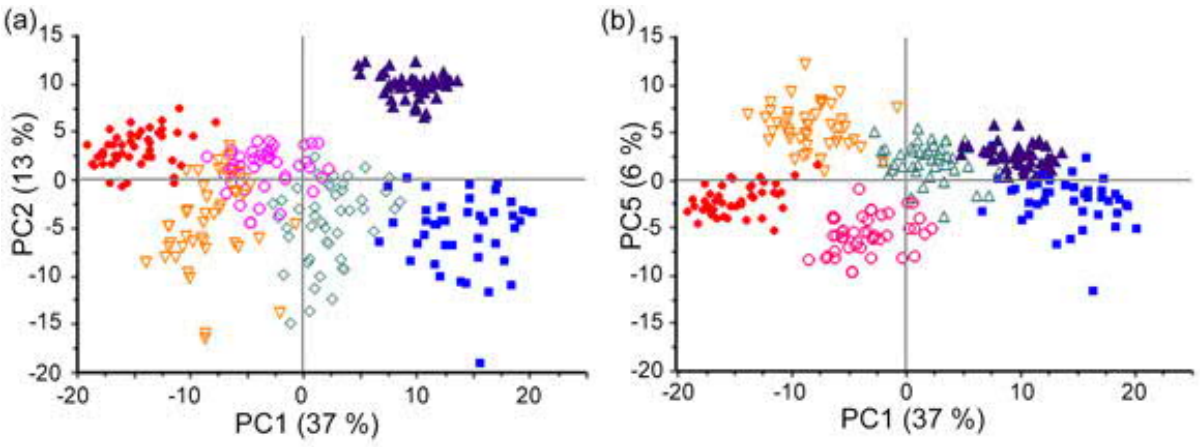

Fig. 8. PCA for monospecies and mixed (1:1) bacterial samples. (a) PCA results plotted according to first two principal components, PC1 and PC2. (b) PCA results plotted according to PC1 and PC5. Blue filled square = *E. coli*, red filled circle= *S. xylosus*, purple filled triangle = *S. enterica*, pink open circle = *E. coli* + *S. xylosus* mixture (1:1), green open diamond = *E. coli* + *S.*

enterica mixture (1:1), and orange inverted triangle = *S. xylosus* and *S. enterica* mixture (1:1) (n = 45 for each sample type).

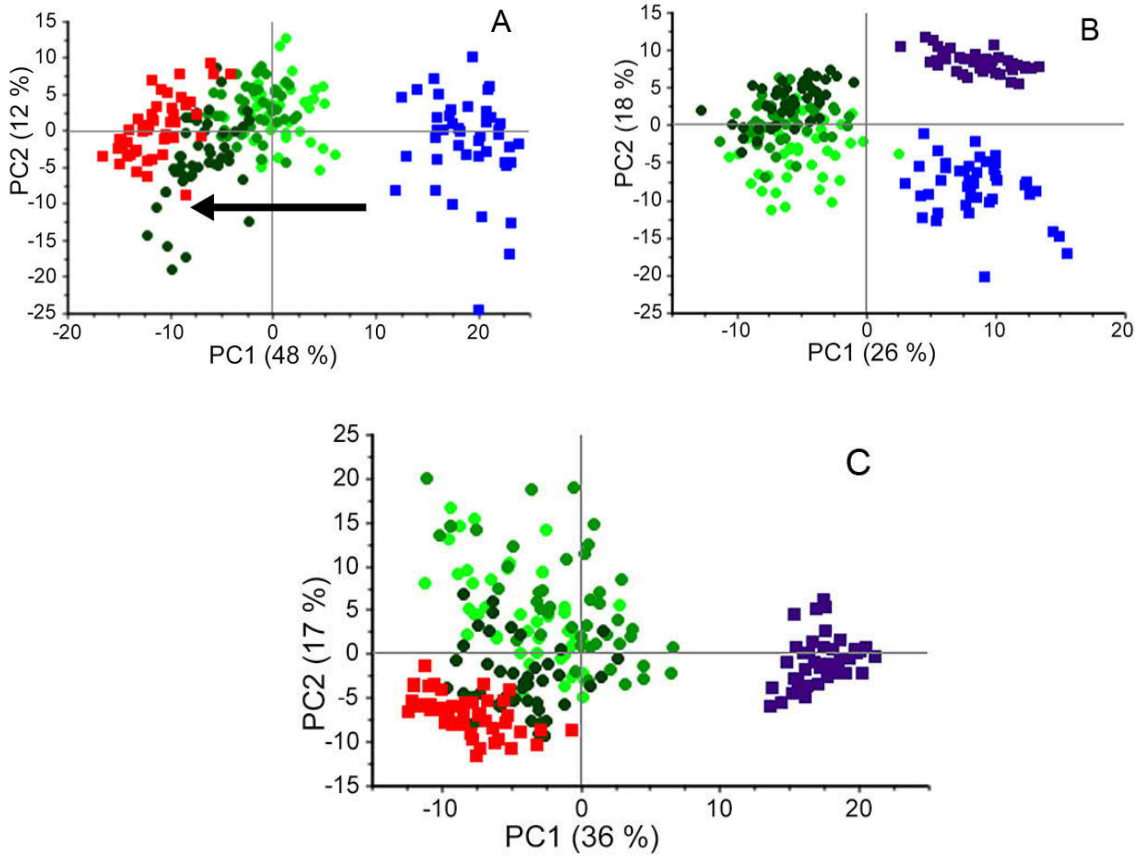

Fig. 9. A: PCA for *E. coli – S. xylosus* mixtures plotted according to the first two PCs. Blue square = *E. coli*, red square= *S. xylosus*, light green filled circle= 1:1 *E. coli – S. xylosus* mixture, green filled circle= 1:2 mixture, dark green filled circle= 1:5 mixture (n = 45 for each sample type). The arrow shows the increasing *S. xylosus* concentration. **B:** PCA for *E. coli – S. enterica* mixtures plotted according to the first two PCs. Blue square = *E. coli*, purple square = *S. enterica*, light green dot = 1 : 1 *E. coli – S. enterica* mixture, green dot = 1 : 2 mixture, and dark green dot =1 : 5 mixture (n = 45 for each sample type). **C:** PCA for *S. xylosus – S. enterica*

mixtures plotted according to the first two PCs. Purple square = *S. enterica*, red square = *S. xylosus*, light green dot = 1 : 1 *S. enterica* – *S. xylosus* mixture, green dot = 1 :2 mixture, and dark green dot = 1 : 5 mixture (n = 45 for each sample type).

Analysis of the monospecies and mixed bacterial samples in various ratios (1:1, 1:2 and 1:5) further confirmed that the monospecies samples can be separated from each other by PCA of their SERS spectra. Mixtures of *E. coli* and *S. xylosus*, *E. coli* and *S. enterica*, and *S. xylosus* and *S. enterica* in addition to the monospecies samples were used. The monospecies samples typically formed own separate clusters, whereas the gradual mixtures showed again heavy overlapping rendering the determination of the composition of mixed samples based on PCA more difficult. Nonetheless, the clustering appeared to monotonously follow the changes in bacterial composition at least to some extent. As shown in Fig. 9A, the *E. coli* – *S. xylosus* mixture clusters appear to position closer and closer to the monospecies *S. xylosus* cluster as the amount of *S. xylosus* in the mixtures increased. Similar gradual change of position of mixed-samples according to the mixture composition was observed also in the other bacterial mixtures (*E. coli* – *S. enterica* and *S. xylosus* – *S. enterica*). The spectra for *E. coli* – *S. enterica*, and *S. xylosus* – *S. enterica* mixtures and respective PCA results are demonstrated in Supplementary Information in Figs S20 - S25 and Fig. 9B-C.

As aforementioned, considered that the density of *E. Coli* in real samples is usually higher than that of either *S. enterica* or *S. xylosus*, we tested the *E. coli* bacteria and *S. xylosus* bacteria with the ratio 10:1 to demonstrate efficiency of PCA analysis in the extreme amounts of *E. Coli* bacteria in the mixture samples. As observed from the Fig. S26 based on the spectra in Fig. S27, the *E-coli-S. xylosus* mixture (10:1 mixing ratio) clusters can be remarkably shifted from the *S. xylosus* cluster region to *E. coli* cluster region. PCA anlaysis results reveal that the mixture with

the ratio of 10:1 can be completely discriminated from the mixture with the ratio 1:1 and two monospecies, proving that the present PCA analysis technology is quite powerful for giving clear differentiation of bacteria mixtures and monospecies.

3.8. SERS spectra of bacteria in soft-drink

To assess the applicability of the recognition of bacteria based on their SERS signals, spectra of bacteria suspended in Fanta soft drink and grown in Fanta were measured. The results were compared to the spectra of the clean control samples. In Fig. 10, the PCA analysis results of *E. coli* and *S. xylosus* in Fanta, and clean *E. coli* and *S. xylosus* reference samples are shown plotted as the function of the first two principal components. The first two PCs cumulatively explain 55% of the total data variance. The bacteria-in-Fanta samples overlapped heavily with the clean samples, which suggests that the bacterial contamination in Fanta can be identified by comparing to the clean reference samples. However, differences in the cluster shape and size suggest some disturbance from Fanta. Therefore, care must be taken when interpreting the results, even though they appear extremely promising. The spectra of *E. coli* in Fanta and *S. xylosus* in Fanta and their mixture in Fanta are shown in Supplementary Information Figs S28 - 32. As shown from the Fig. 10, as far as mixture of *E.coli* and *S. xylosus* with ratio 1:1 is concerned, although the mixed sample in Fanta cannot be well overlapped with the sample containing water-suspended bacteria. Both suspended mixture samples (in Fanta and water), can be diffentiated from monospecies, indicating that it is possible to recognize the bacterial mixture in Fanta soft drink.

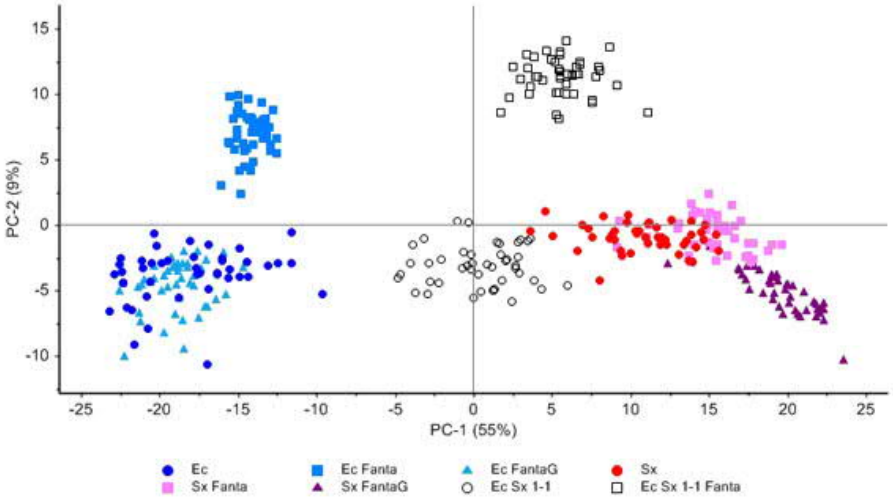

Fig. 10. PCA of monospecies bacteria and the same bacteria and their mixture species in Fanta soft drink. Blue filled circle = *E. coli*, blue filled triangle = *E. coli* grown in Fanta to LB nutrient 1：10，blue filled box = *E-coli* suspended in Fanta, red filled circle = *S. xylosus*, pink filled box = *S. xylosus* suspended in Fanta, purple filled triangle = *S.xylosus* grown in Fanta to LB nutrient 1：10, black empty circle = mixture of *E-coli* and *S. xylosus* with the ratio of 1:1, black empty circle = mixture of *E-coli* and *S.xylosus* with the ratio of 1:1 suspended in Fanta. (n = 45 for each sample type).

4. Conclusions

We have demonstrated that a 3D bio-inorganic scaffold of Ag nanoplate aggregate--bacteria - Au@Ag vertical nanorod supercrystal (NBNS), as a model of combined plasmonic enhancement from asymmetric nanoparticles and assembly, can be fabricated via layer-by-layer patterning. Antibiotics vancomycin was shown to increase the robustness of the scaffold when introduced into the top layer of the nanorod supercrystal. Inherently weak Raman signal was dramatically enhanced by aid of synergistic plasmonic enhancing effect from both plasmonic nanoplates

aggregate and nanorod supercrystal, enabling discrimination of Gram+ and Gram- bacteria including *E. coli*, *S. enterica* and *S. xylosus* based on their SERS spectra. PCA analysis of the SERS spectra collected from monospecies and mixed bacteria samples demonstrated that Gram+ and Gram- bacteria can be clearly differentiated; moreover, the mixed bacteria can also be discriminated. For different mixing ratios of two bacteria, a regular shift in PCA analysis following the changes in the ratio, was obtained. Importantly, the feasibility of the method for food quality analysis was demonstrated via detection of bacteria embedded in a soft drink. It can be expected that the hybridized scaffold of nanoaggregate and supercrystal can be utilized as a highly-sensitive optical nanosensor.

ASSOCIATED CONTENT

Supporting Information. Further experimental details, UV-Vis-NIR spectra, SEM images, all the SERS spectra behind the statistical analysis, AFM images, PCA analysis. This material is available free of charge via Internet.

AUTHOR INFORMATION

Corresponding Author

* Corresponding author. Emails: jwang@iim.cas.cn; gehonghua@gmail.com; j.jussi.toppari@jyu.fi

Author Contributions

The manuscript was written through contributions of all authors. All authors have given approval to the final version of the manuscript. ‡These authors contributed equally.

Funding Sources

MOST China-Finland International Cooperation Project (Grant No. 2014DFG42290)

Tekes – the Finnish Funding Agency for Innovation (Project No. 1185/31/2013 and 1191/31/2013)

National Natural Science Foundation of China (Grant Nos. 31270770, 31400641, 21077106)

ACKNOWLEDGMENT

This work is supported by MOST China-Finland International Cooperation Project (Grant No. 2014DFG42290) and Tekes – the Finnish Funding Agency for Innovation (Project No. 1185/31/2013 and 1191/31/2013), the National Natural Science Foundation of China (Grant Nos. 31270770, 21077106). BioNavis, Fimlab Laboratories, PBL Brewing Laboratory (VTT) and Orion Diagnostica are gratefully acknowledged. Biocenter Finland is acknowledged for

infrastructure support. Dr Meng Fu and JieHong Mao from Merieux NutriSciences-Sino Analytica (QingDao and NingBo) company is gratefully acknowledged.

ABBREVIATIONS

SERS, surface enhanced raman spectroscopy; LSPR, localized surface plasmon resonance; NBNS, nanoplate-bacteria-nanorod supercrystal;

REFERENCES

[1] C. Bernabini., D. Holmes, H. Morgan, Micro-impedance cytometry for detection and analysis of micron-sized particles and bacteria. Lab. Chip 11 (2011) 407-412.

[2] N. Couniot, L. A. Francis., D. Flandre., Resonant dielectrophoresis and electrohydrodynamics for high-sensitivity impedance detection of whole-cell bacteria. Lab. Chip 15 (2015) 3183-3191.

[3] S. Wang, A. K. Singh, D. Senapati, A. Neely, H. Yu., P.C. Ray, Rapid Colorimetric Identification and Targeted Photothermal Lysis of Salmonella Bacteria by Using Bioconjugated Oval-Shaped Gold Nanoparticles. Chem. Eur. J. 16 (2010) 5600-5606.

[4] M. S. Verma, P. Z. Chen, L. Jones, F. X. Gu, Branching and size of CTAB-coated gold nanostars control the colorimetric detection of bacteria. RSC. Adv. 4 (2014) 10660-10668.

[5] M. S. Mannoor, S. Zhang, A. J. Link, M. C. McAlpine, Electrical detection of pathogenic bacteria via immobilized antimicrobial peptides. PNAS. 107 (2010) 19207–19212.

[6] Y. Chen, Z. P. Michael, G. P. Kotchey, Y. Zhao, A. Star, Electronic Detection of Bacteria Using Holey Reduced Graphene Oxide. ACS Applied Materials & Interfaces. 6 (2014) 3805–3810.

[7] G. Feng, Y. Yuan, H. Fang, R. Zhang, B. Xing, G. Zhang, D. Zhang, B. Liu, A light-up probe with aggregation-induced emission characteristics (AIE) for selective imaging, naked-eye detection and photodynamic killing of Gram-positive bacteria. Chem. Commun. 51 (2015) 12490-12493.

[8] J. Wang, M. J. Morton, C. T. Elliott, N. Karoonuthaisiri, L. Segatori, S. L. Biswal, Rapid detection of pathogenic bacteria and screening of phage-derived peptides using microcantilevers. Anal. Chem.86 (2014) 1671-1678.

[9] M. H. Abdalhai, A. Fernandes, M. Bashari, J. Ji, Q. He, X. Sun, Rapid and sensitive detection of foodborne pathogenic bacteria (Staphylococcus aureus) using an electrochemical DNA genomic biosensor and its application in fresh beef. J. Agric. Food. Chem. 62 (2014) 12659-12667.

[10] R. Pacheco-Gómez, J. Kraemer, S. Stokoe, H. England, C. Penn, E. Stanley, A. Rodger, J. Ward, M. Hicks, T. Dafforn, Detection of pathogenic bacteria using a homogeneous immunoassay based on shear alignment of virus particles and linear dichroism. Anal. Chem. 84 (2012) 91-97.

[11] J. Chang, S. Mao, Y. Zhang, S. Cui, G. Zhou, X. Wu, C. H. Yang, J. Chen, Ultrasonic-assisted self-assembly of monolayer graphene oxide for rapid detection of Escherichia coli bacteria. Nanoscale. 9 (2013) 3620-3626.

[12] T. J. Ondera, A. T. HammeII, A gold nanopopcorn attached single-walled carbon nanotube hybrid for rapid detection and killing of bacteria. J. Mater. Chem. B. 43 (2014) 7534-7543.

[13] F. Cui, Z. Q. Hu, M. Azlin, M. S. Lin, Rapid detection of food- and waterborne bacteria using surface-enhanced Raman spectroscopy coupled with silver nanosubstrates. Appl. Microbiol. Biotechnol. 92 (2011) 1053-1061.

[14] A. Sivanesan, E. Witkowska, W. Adamkiewicz, L. Dziewit, A. Kamińska, J. Waluk, Nanostructured silver–gold bimetallic SERS substrates for selective identification of bacteria in human blood. Analyst. 139 (2014), 1037-1043.

[15] D. Yang, H. Zhou, C. Haisch, R. Niessner, Y. Ying, Reproducible E. coli detection based on label-free SERS and mapping. Talanta. 146 (2016) 457-463.

[16] H. Zhou, D. Yang, N. P. Ivleva, N. E. Mircescu, R. Niessner, C. Haisch, SERS Detection of Bacteria in Water by in Situ Coating with Ag Nanoparticles. Anal. Chem. 86 (2014) 1525-1533.

[17] X. Wu, C. Xu, R. A. Tripp, Y. W. Huang, Y. Zhao, Detection and differentiation of foodborne pathogenic bacteria in mung bean sprouts using field deployable label-free SERS devices. Analyst. 138 (2013) 3005-3012.

[18] Y. Zhao, X. Yang, H. Li, Y. Luo, R. Yu, L. Zhang, Y. Yanga, Q. Song, Au nanoflower–Ag nanoparticle assembled SERS-active substrates for sensitive MC-LR detection. Chemical Communications. 51 (2015) 16908-16911.

[19] C. Zhu, G. Meng, Q. Huang, Z. Zhang, Q. Xu, G. Liu, Z. Huang, Z. Chu, Ag nanosheet-assembled micro-hemispheres as effective SERS substrates Chemical Communications. 47 (2011) 2709-2711.

[20] X. Wang, D. Yang, P. Huang, M. Li, C. Li, D. Chen, D. Cui, Hierarchically assembled Au microspheres and sea urchin-like architectures: formation mechanism and SERS study. Nanoscale. 4 (2012) 7766-7772.

[21] S. Gómez-Graña, C. Fernández-López, L. Polavarapu, J. B. Salmon, J. Leng, I. Pastoriza-Santos, J. Pérez-Juste, Gold Nanooctahedra with Tunable Size and Microfluidic-Induced 3D Assembly for Highly Uniform SERS-Active Supercrystals. Chemistry of Materials. 27 (2015) 8310-8317.

[22] P. Alonso-Gonzalez, M. Schnell, P. Sarriugarte, H. Sobhani, C. H. Wu, N. Arju, A. Khanikaev, F. Golmar, P. Albella, L. Arzubiaga, F. Casanova, L. E. Hueso, P. Nordlander, G. Shvets, R. Hillenbrand, Real-Space Mapping of Fano Interference in Plasmonic Metamolecules. Nano. Lett. 11 (2011) 3922-3926.

[23] P. J. De Groot, G. J. Postma., W. J. Melssen., L. M. C. Buydens, V. Deckert, R. Zenobi, Application of principal component analysis to detect outliers and spectral deviations in near-field surface-enhanced Raman spectra. Anal. Chim. Acta. 446 (2001) 71-83.

[24] Å. Rinnan, F. Van den Berg, S. Balling Engelsen, Review of the most common pre-processing techniques for near-infrared spectra. *TrAC,* Trends Anal. Chem. 28 (2009) 1201-1222.

[25] G. Das, F. Gentile, M. L. Coluccio, A. M. Perri, A. Nicastri, F. Mecarini, G. Cojoc, P. Candeloro, C. Liberale, F. D. Angelis, E. D. Fabrizio, Principal component analysis based methodology to distinguish protein SERS spectra. J. Mole. Struct. 993 (2011) 500-505.

[26] R. Goodacre, E. M. Timmins, R. Burton, N. Kaderbhai, A. M. Woodward, D. B. Kell, P. J. Rooney, Rapid identification of urinary tract infection bacteria using hyperspectral whole-organism fingerprinting and artificial neural networks. Microbiology. 144 (1998) 1157-1170.

[27] S. Gómez-Graña, J. Pérez-Juste, R. A. Alvarez-Puebla, A. Guerrero-Martínez, L. M. Liz-Marzán, Self-assembly of Au@Ag nanorods mediated by gemini surfactants for highly efficient SERS-active supercrystals. Adv. Optical. Mater. 1 (2013) 477-481.

[28] P. J. Yunker, T. Still, M. A. Lohr, A. G. Yodh, Suppression of the coffee-ring effect by shape-dependent capillary interactions. Nature. 476 (2011) 308-311.

[29] X. Lv, W. Ge, Q. Li, Y. Wu, H. Jiang, X. Wang, Rapid and Ultrasensitive Electrochemical Detection of Multidrug-Resistant Bacteria Based on Nanostructured Gold Coated ITO Electrode. ACS Applied Materials & Interfaces. 6 (2014) 11025-11031.

[30] H. J. Chung, T. Reiner, G. Budin, C. Min, M. Liong, D. Issadore, H. Lee, R. Weissleder, Ubiquitous Detection of Gram-Positive Bacteria with Bioorthogonal Magnetofluorescent Nanoparticles. ACS Nano. 5 (2011) 8834-8841.

[31] M. Schafer, T. R. Schneider, G. M. Sheldrick, Crystal Structure of Vancomycin. Structure. 4 (1996) 1509-1515.

[32] P. J. Loll, A. Derhovanessian, M. V. Shapovalov, J. Kaplan, L. Yang, P. H. Axelsen, Vancomycin Forms Ligand-Mediated Supramolecular Complexes. J. Mol. Biol. 385 (2009) 200-211.

[33] J. E. Millstone, S. J. Hurst, G. S. Metraux, J. I. Cutle, C. A. Mirkin,Colloidal Gold and Silver Triangular Nanoprisms. Small. 5 (2009) 646-664.

[34] G. K. Joshi, P. J. McClory, S. Dolai, R. Sardar, Improved localized surface plasmon resonance biosensing sensitivity based on chemically-synthesized gold nanoprisms as plasmonic transducers. J. Mater. Chem. 22 (2012) 923-931.

[35] S. H. Ciou, Y. W. Cao, H. C. Huang, D. Y. Su, C. L. Huang, SERS Enhancement Factors Studies of Silver Nanoprism and Spherical Nanoparticle Colloids in The Presence of Bromide Ions. J. Phys. Chem. C. 113 (2009) 9520-9525.

[36] B. Aoune, D. M. Zhang, T. Felicia, J. H. Naomi, Surface-Enhanced Raman Spectroscopy of DNA. J. Am. Chem. Soc. 16 (2008) 5523-5529.

[37] L. Yilin, H. Qing, M. Guowen, L. J. Wu, J. Zhang, Label-free selective SERS detection of PCB-77 based on DNA aptamer modified SiO_2@Au core/shell nanoparticles. Analyst. 139 (2014) 3083-3087.

Supporting Information

Synergistic enhancement via plasmonic nanoplate-bacteria-nanorod supercrystals for highly efficient SERS sensing of food-borne bacteria

WeiQiang Wang[‡a], Ville Hynninen[‡b], Li Qiu[‡c], AiWen Zhang[c], Tibebe Lemma[d], NanNan Zhang[a], HongHua Ge[*a], J. Jussi Toppari[*d], Vesa P. Hytönen[b] and Jin Wang[*a]

[a] *Institute of Health Sciences and School of Life Science, AnHui University, Hefei, Anhui 230601, P.R. China*

[b] *BioMediTech, University of Tampere, FI-33520 Tampere, Finland and Fimlab Laboratories, FI-35520, Tampere, Finland*

[c] *Institute of Intelligent Machines, Chinese Academy of Sciences, Hefei, Anhui 230031, P. R. China*

[d] *University of Jyväskylä, Department of Physics, Nanoscience Center, P.O. Box 35, FI-40014, University of Jyväskylä, Finland*

‡ These authors contributed equally to this work.

* Corresponding author. Emails: jwang@iim.cas.cn; gehonghua@gmail.com, j.jussi.toppari@jyu.fi

Experimental details

S1.1. Synthesis of Au@Ag core shell nanorods (Au@Ag NRs)

AuNRs could be synthesized by modified seed-mediated approach [1]. Firstly, 10 mL 0.5 mM $HAuCl_4$ was mixed with 10 mL 0.2 M CTAB. Subsequently, 600 µL 0.02 M ice-cold $NaBH_4$ was added to the mixed solution. Vigorous stirring of the seed solution was kept going for 2min, and was subsequently settled at room temperature for 1h. Secondly, 50 mL 0.2 M CTAB, 2.5 mL 4 mM $AgNO_3$, 50 mL 1 mM $HAuCl_4$ were mixed as a growth solution, followed by addition of 700 µL of 0.08 M vitamin C. Finally, the AuNRs were prepared by addition of 120 µL seed solution to the growth solution. The as–prepared AuNRs were centrifuged and redispersed in 10 mL Milli-Q water.

2 mL AuNRs solution was diluted into 10 mL 0.1 M CTAB aqueous solution. 0.5 mL 4 mM $AgNO_3$ solution, 600 µL 0.1 M vitamin C, 1.2 mL 0.1 M NaOH solution were added to the solution. During this step, the color of solution was changed from yellow-reddish to green, indicating formation of silver shell. The as–prepared bimetallic Au@Ag core-shell nanorods were centrifuged and redispersed in 1 mL Milli-Q water.

S1.2. Synthesis of Ag nanoplate

Ag nanoplates were synthesized via seed-mediated method [2]. As an initial step, 5mL of 2.5 mM $NaCA_3$ was mixed with a mixture prepared by combining 0.25 mL 500 mg/L PSS and 0.3mL 10mM $NaBH_4$. Subsequently, 5mL of 0.5 mM $AgNO_3$ was added to the mixture with a rate of 2mL/min under constant stirring to obtain the Ag seed solution. As the second step, 75µL 10 mM ascorbic acid was added to 5 mL H_2O and various amounts of seed solution was added (40 µL ~ 400µL), followed by addition of 3 mL 0.5 mM $AgNO_3$ with a rate of 1mL/min to form Ag nanoplates.

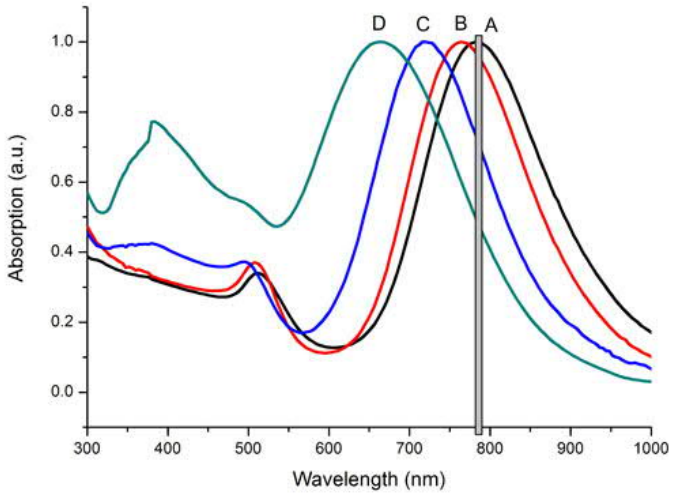

Fig. S1. Normalized UV/Vis/NIR spectra of (A) Au nanorods with LSPR band at 783 nm; (B) Au@Ag core-shell nanorods with LSPR band at 765 nm; (C) Au@Ag core-shell nanorods with LSPR band at 720 nm; (D) Au@Ag core-shell nanorods with LSPR band at 664 nm. The gray line means laser line exciation at 785 nm. The amounts of the deposited Ag and thus the shell thickness increases from B to D.

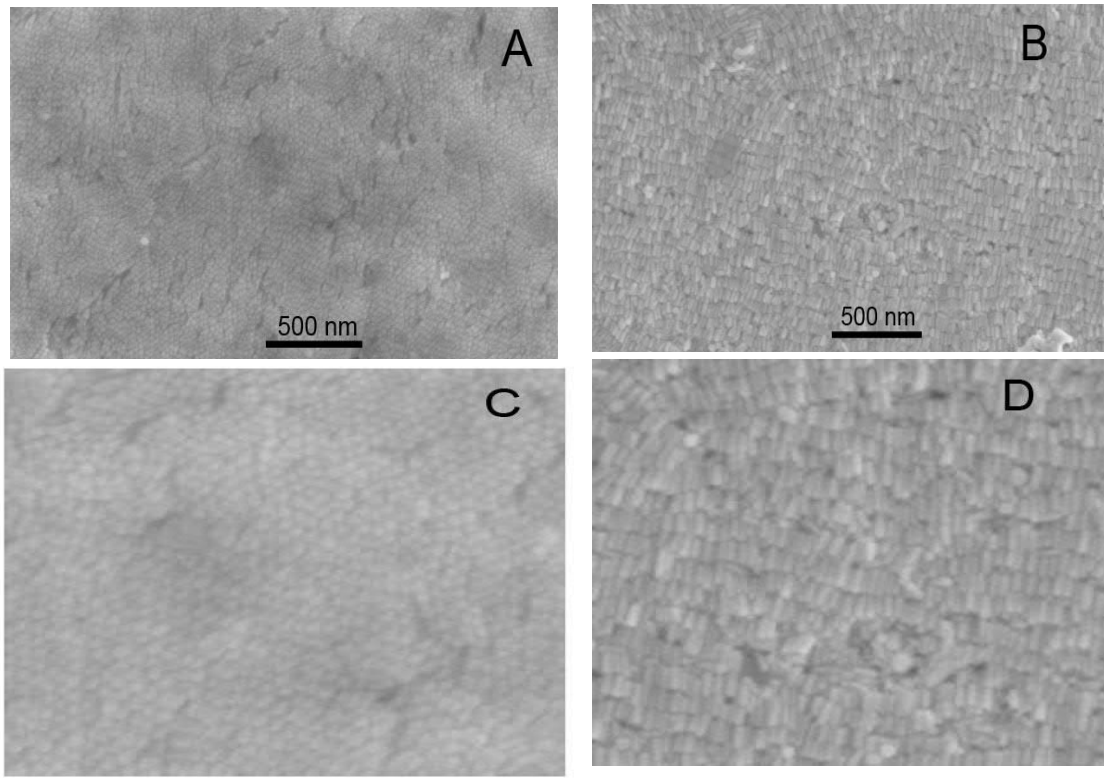

Fig. S2. SEM images of A: plasmonic vertical nanorod supercrystal; B: plasmonic parallel nanorod supercrystal; C: expansion of plasmonic vertical nanorod supercrystal; D: expansion of plasmonic parallel nanorod supercrystal.

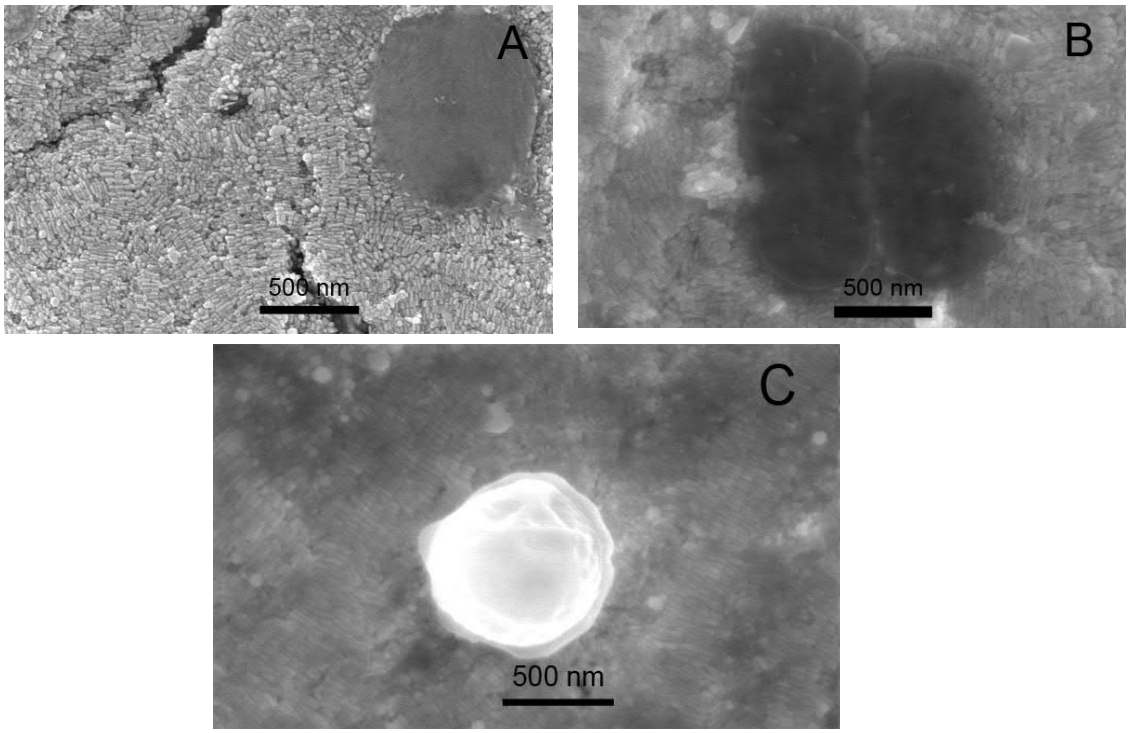

Fig. S3. SEM images of bacteria attached on the parallel supercrystal of plasmonic nanorods. A: *E. coli*; B: *S. enterica*; C: *S. xylosus*

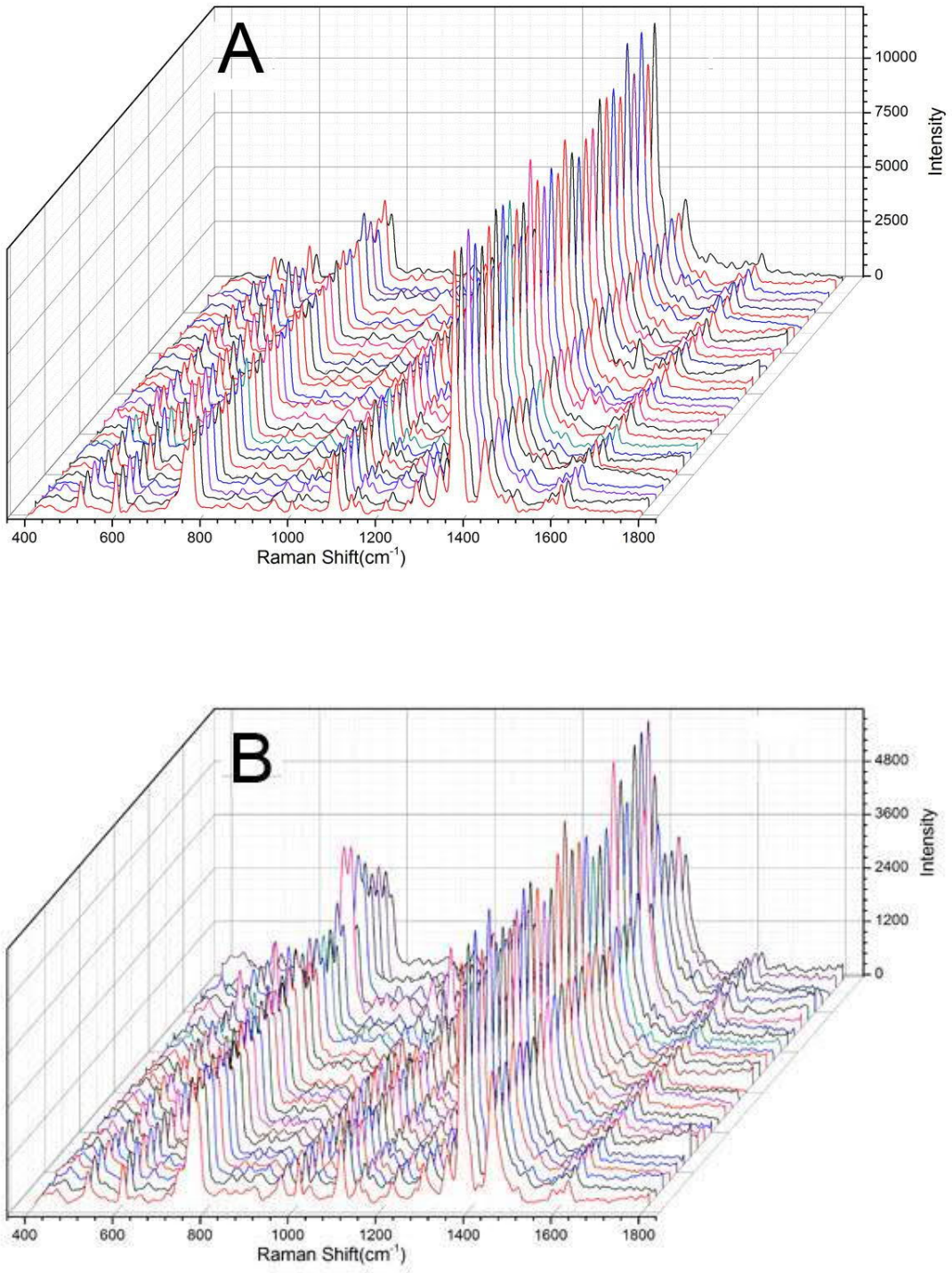

Fig. S4. Point-to-point collected SERS spectra of 2-quinolinethiol (2-QT) on A: a plasmonic vertical nanorod supercrystal, B: parallel nanorod supercrystal

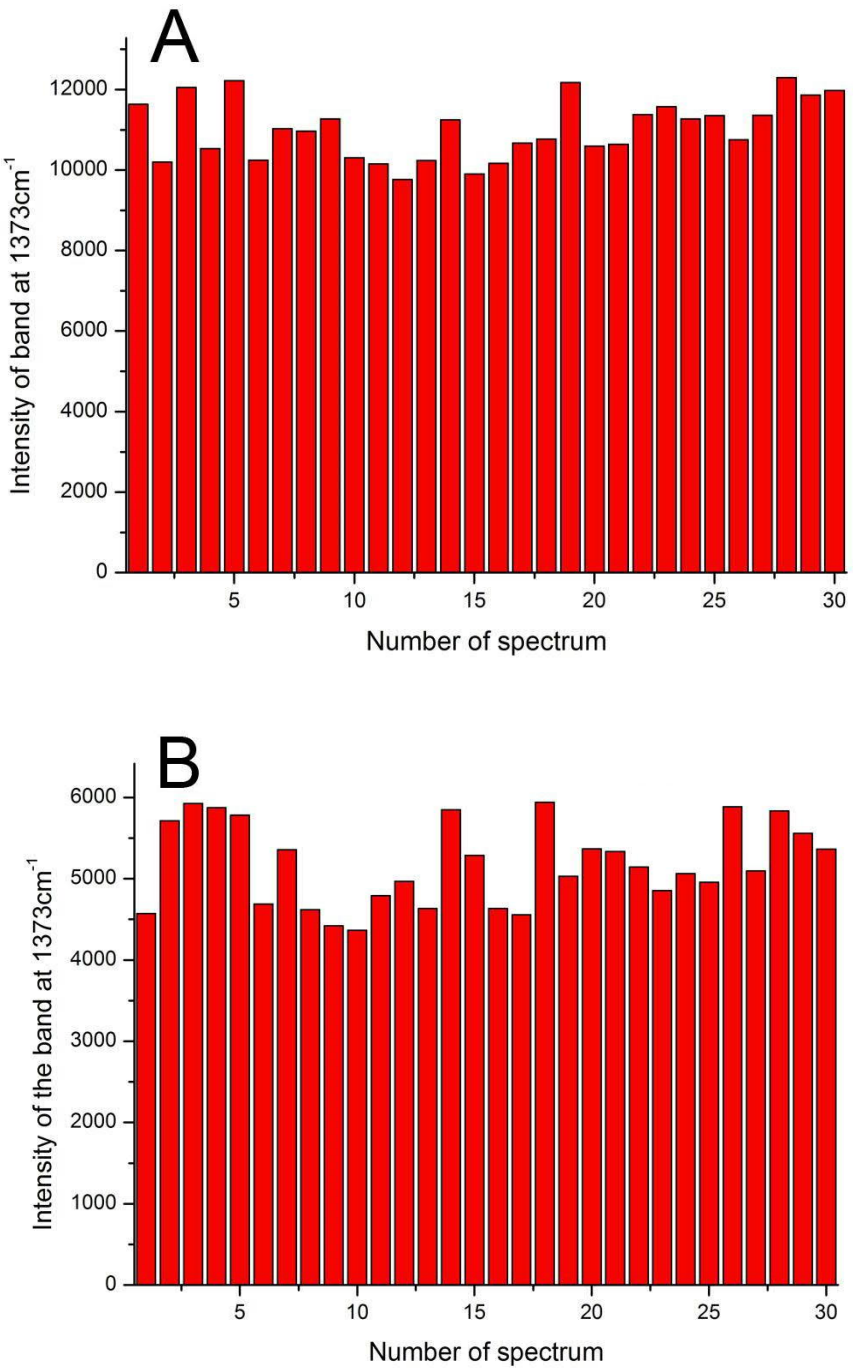

Fig. S5. Variation of SERS intensity of 2-quinolinethiol (2-QT) on A: plasmonic vertical nanorod supercrystal, B: parallel nanorod supercrystal

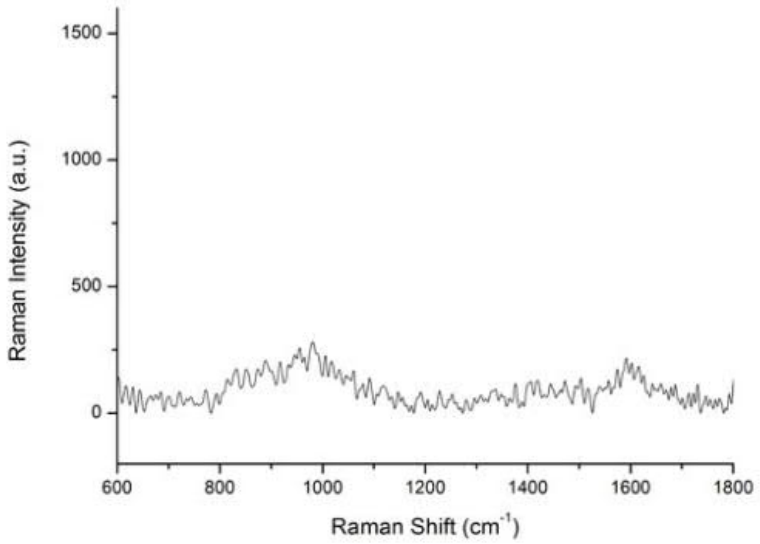

Fig. S6. SERS spectra of vancomycin-coated nanorod supercrystal.

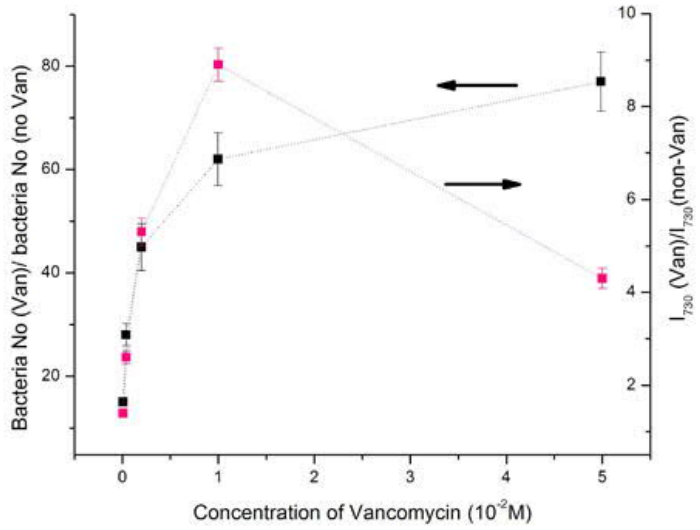

Fig. S7. Bacteria absorption efficiency and SERS sensitivity of vancomycin-coated 3D nanorod supercrystal as a function of vancomycin concentration ($5x10^{-2}$M, $1x10^{-2}$M, $0.2x10^{-2}$M, $0.04x10^{-2}$M, and $0.008x10^{-2}$M).

The number of bacteria immobilized on NBNS substrate is normalized by that on the substrate without vancomycin coating to give estimation of bacteria absorption efficiency. I_{730} SERS intensity of *S.xylosus* bacteria on NBNS substrate is normalized by that the substrate without vancomycin coating to show its relative SERS intensity.

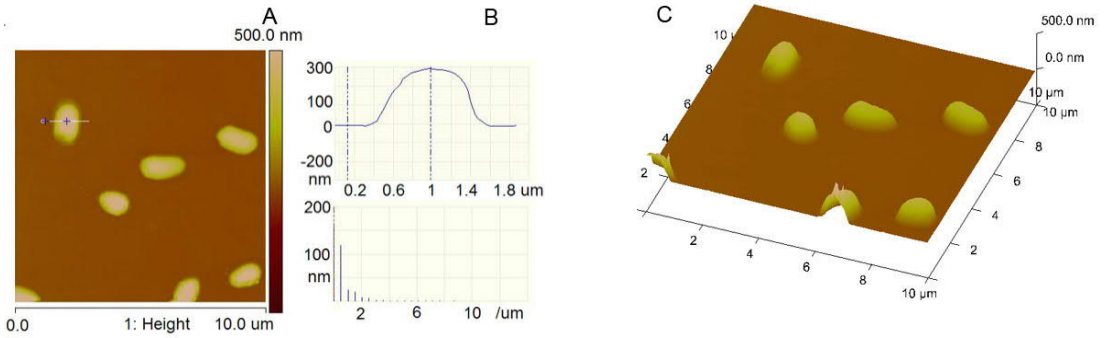

Fig. S7. (A) AFM image of *E. coli* on a silicon chip; (B) The height of *E. coli* on a silicon chip; (C) 3D AFM image of *E. coli* on a silicon chip

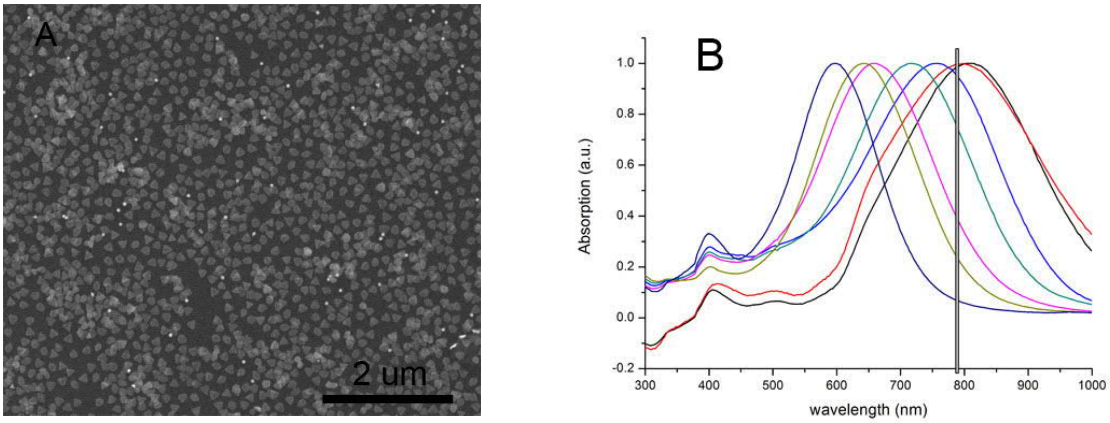

Fig. S8. A: SEM images of Ag nanoplate, B: Extinction profile of Ag nanoplates with tunable LSPR band. The strong band located at 750~800 nm in the near-infrared region was selected for assembling the 3D scaffold. The gray line shows the excitation laser line at 785 nm.

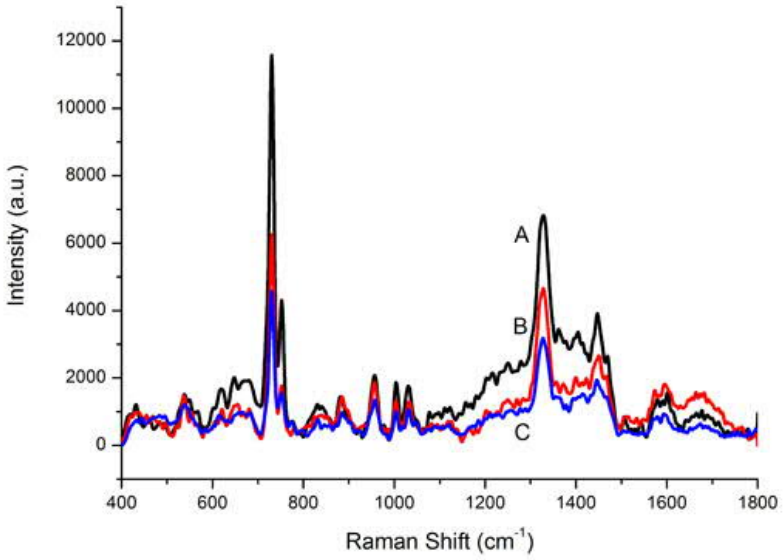

Fig. S9. SERS spectra of *S. xylosus* on different substrate. A: Ag nanoplate aggregate-*S. xylosus*-vancomycin-coated Au@Ag core-shell nanorod supercrystal; B: mixture of *S. xylosus* and Ag nanoplates; C: vancomycin-coated Au@Ag core-shell nanorod supercrystal

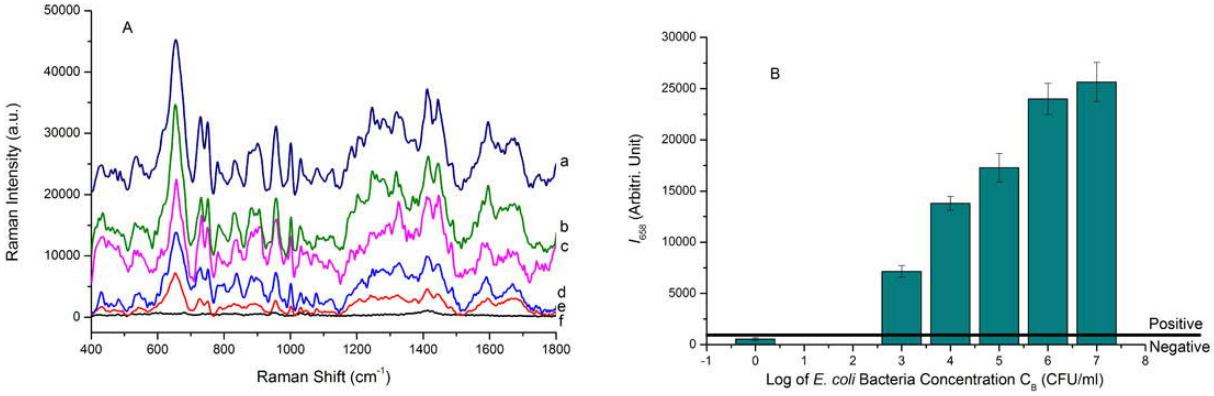

Fig. S10. (A): The SERS spectra of *E. coli* (a-e corresponding to C_B = 10^7, 10^6, 10^5, 10^4, 10^3 CFU/mL, f corresponding to Milli-Q water on the identical SERS substrate. (B) The mean and standard deviation of the SERS peak intensity I_{658} of E-Coli at the different concentrations C_B = 10^7, 10^6, 10^5, 10^4, 10^3 CFU/mL and Milli-Q water.

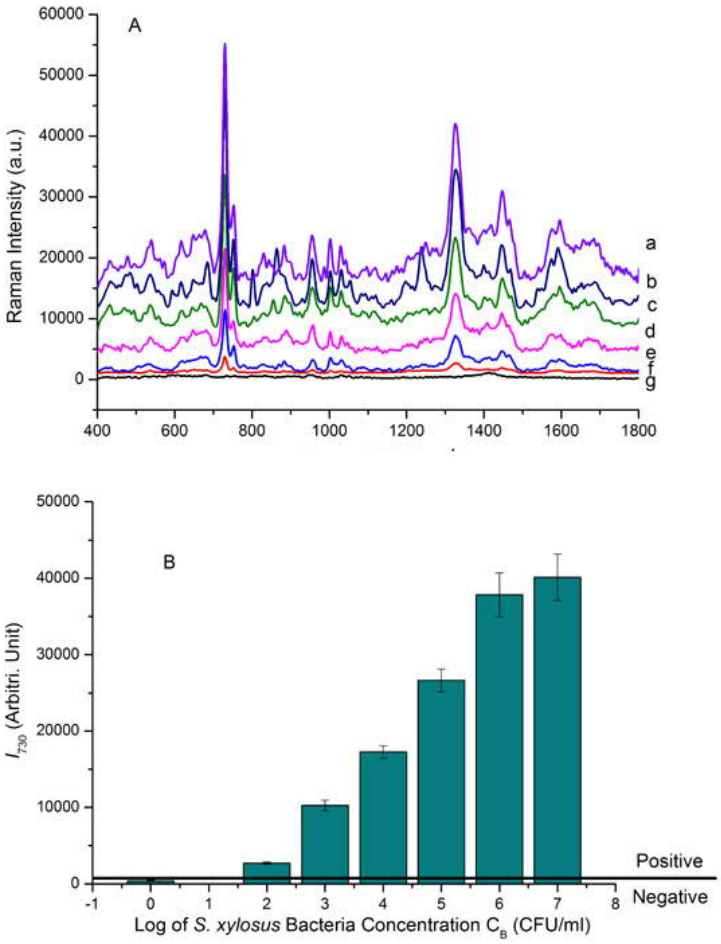

Fig. S11. (A): The SERS spectra of *S. xylosus* (a-f corresponding to C_B = 10^7, 10^6, 10^5, 10^4, 10^3 ,10^2 CFU/mL, f corresponding to Milli-Q water on the identical SERS substrate. (B) The mean and standard deviation of the SERS peak intensity I_{730} of *S.xylosus* at the different concentrations C_B = 10^7, 10^6, 10^5, 10^4, 10^3,10^2 CFU/mL and Milli-Q water.

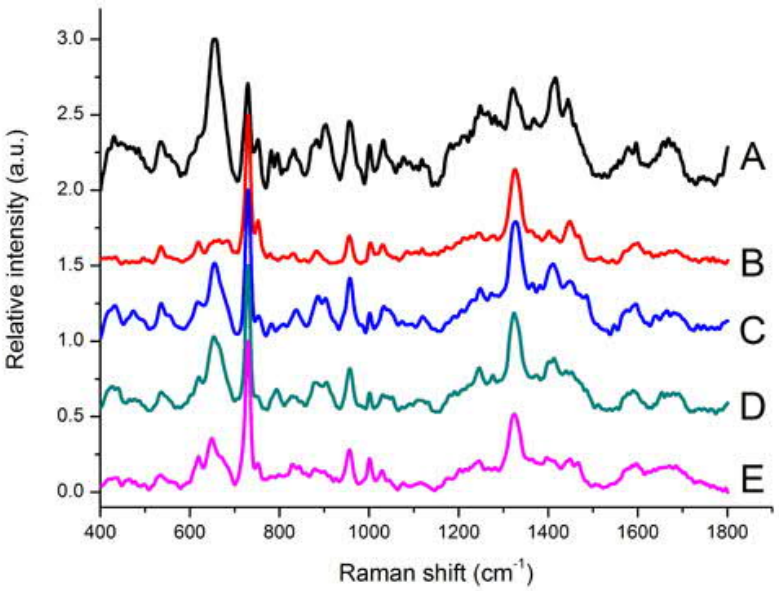

Fig. S12. A comparison on normalized SERS spectra of the mixed and monospecies bacteria collected from a 3D plasmonic nanoplates aggregate-bacteria-vertical nanorod supercrystal. A: Gram- *E. coli*; B: Gram+ *S. xylosus*; C: mixture of *E. coli* and *S. xylosus* with ratio 1:1; D: mixture of *E. coli* and *S. xylosus* with ratio 1:2; E: mixture of *E. coli* and *S. xylosus* with ratio 1:5.

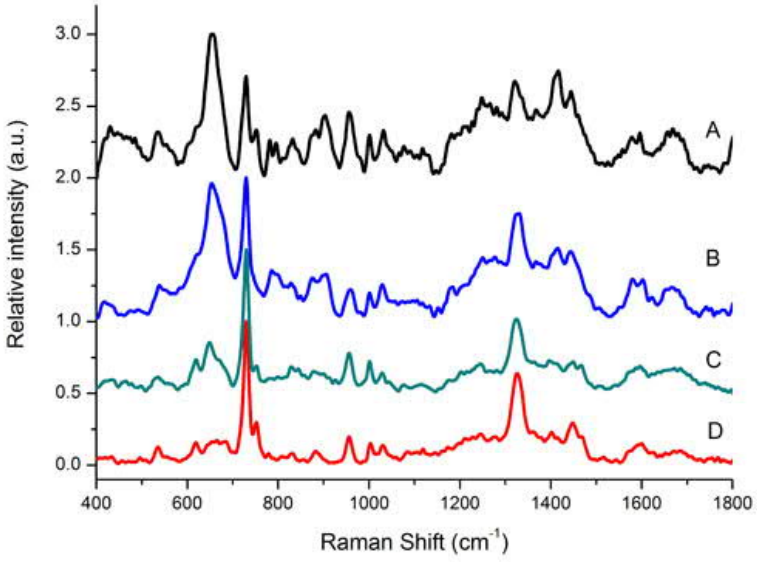

Fig. S13. A comparison on normalized SERS spectra of the mixed and monospecies bacteria collected from a 3D plasmonic nanoplates aggregate-bacteria-vertical nanorod supercrystal. A: Gram- *E. coli*; B: mixture of *E. coli* and *S. xylosus* with ratio 10:1; C: mixture of *E. coli* and *S. xylosus* with ratio 1:1; D: Gram+ *S. xylosus.*

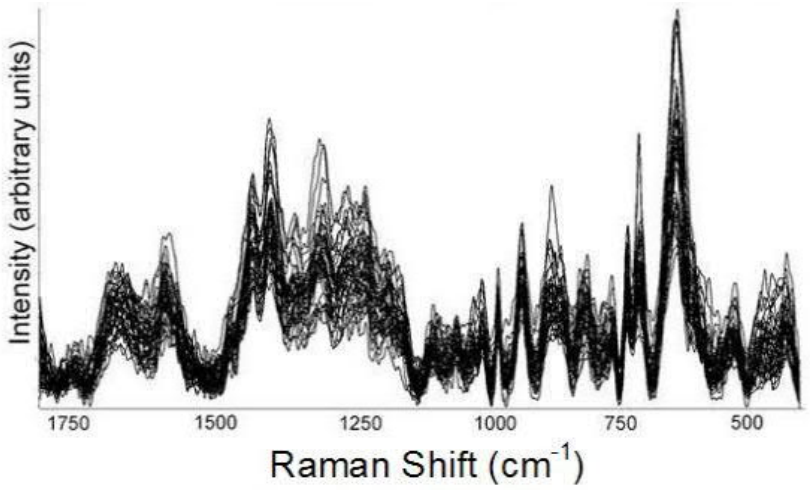

Fig. S14. Linear baseline corrected SERS spectra of *E. coli*. 400 cm^{-1}~1800 cm^{-1} range; n = 45.

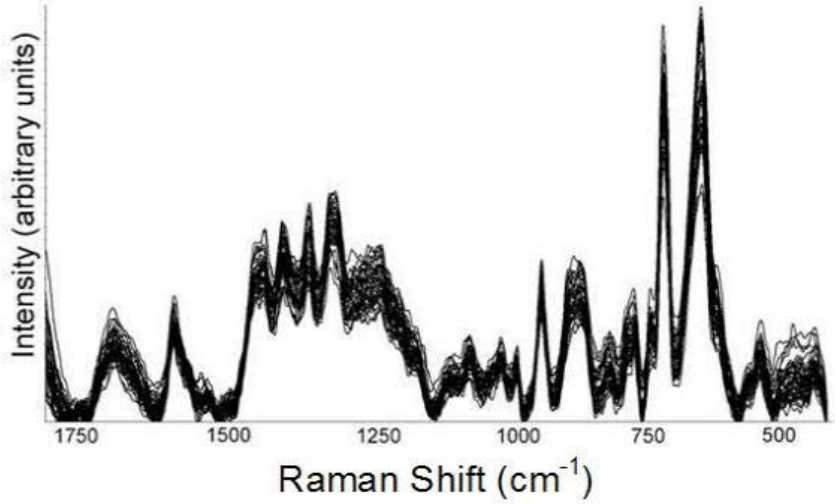

Fig. S15. Linear baseline corrected SERS spectra of *S. enterica*. 400 cm^{-1}~1800 cm^{-1} range; n = 45.

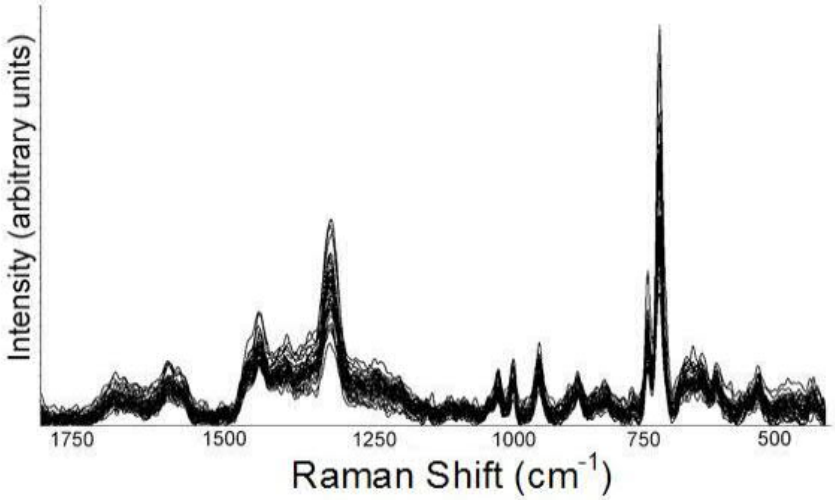

Fig. S16. Linear baseline corrected SERS spectra of *S. xylosus*. 400 cm^{-1}~1800 cm^{-1} range; n = 45.

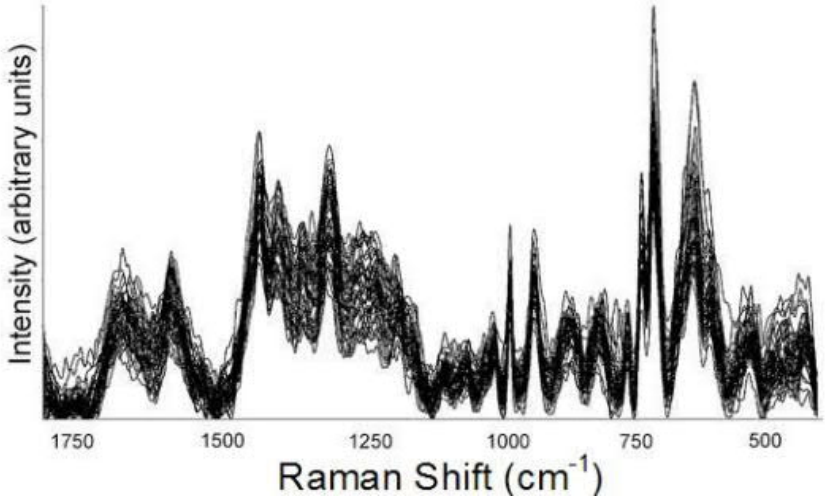

Fig. S17. Linear baseline corrected SERS spectra of 1:1 *E. coli* – *S. enterica* mixture. 400 cm^{-1} ~1800 cm^{-1} range; n = 45.

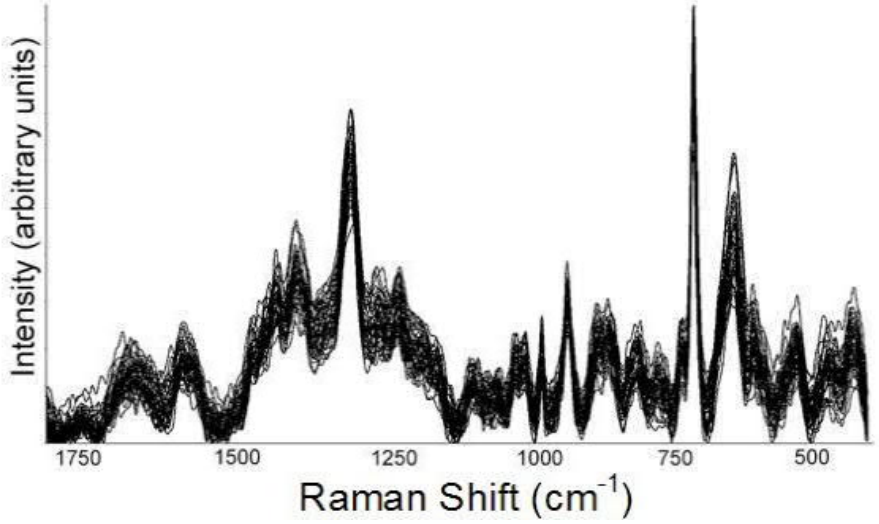

Fig. S18. Linear baseline corrected SERS spectra of 1:1 *E. coli* – *S. xylosus* mixture. 400 cm^{-1} ~1800 cm^{-1} range; n = 45.

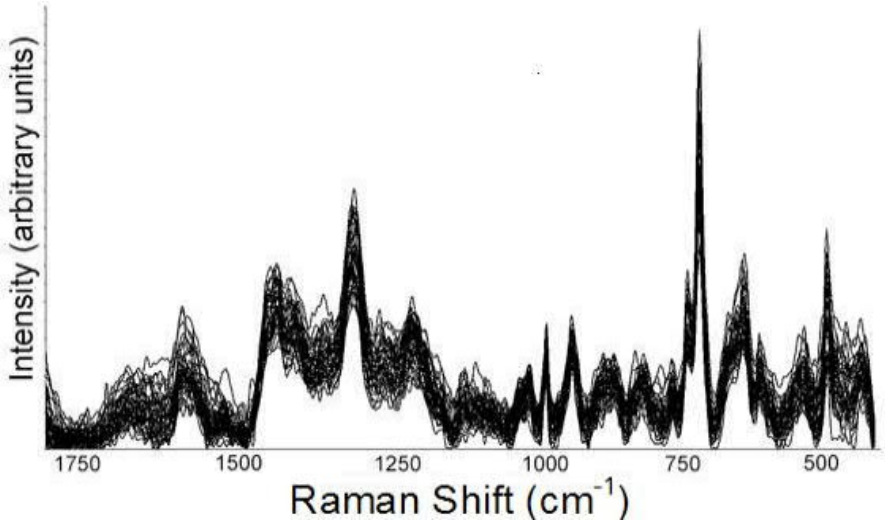

Fig. S19. Linear baseline corrected SERS spectra of 1:1 *S. enterica* – *S. xylosus* mixture. 400 cm^{-1}-1800 cm^{-1} range; n = 45.

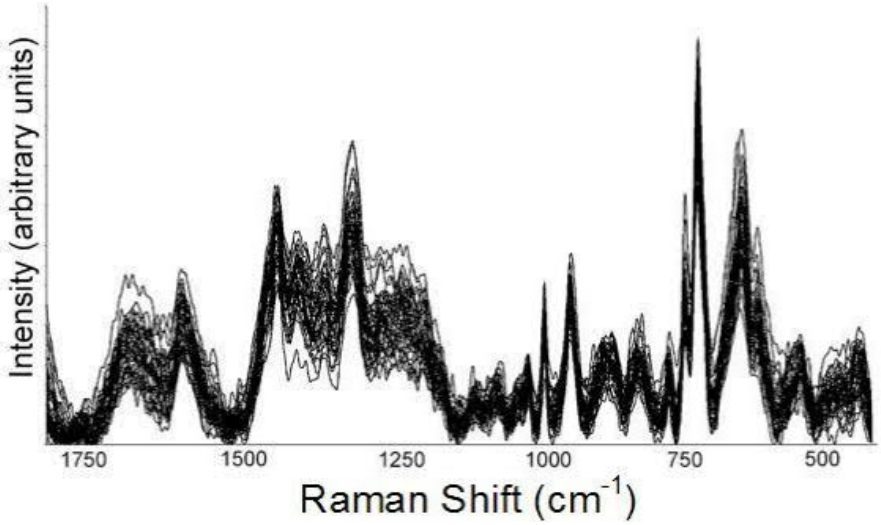

Fig. S20. Linear baseline corrected SERS spectra of 1:2 *E. coli* – *S. enterica* mixture. 400 cm^{-1} ~1800 cm^{-1} range; n = 45.

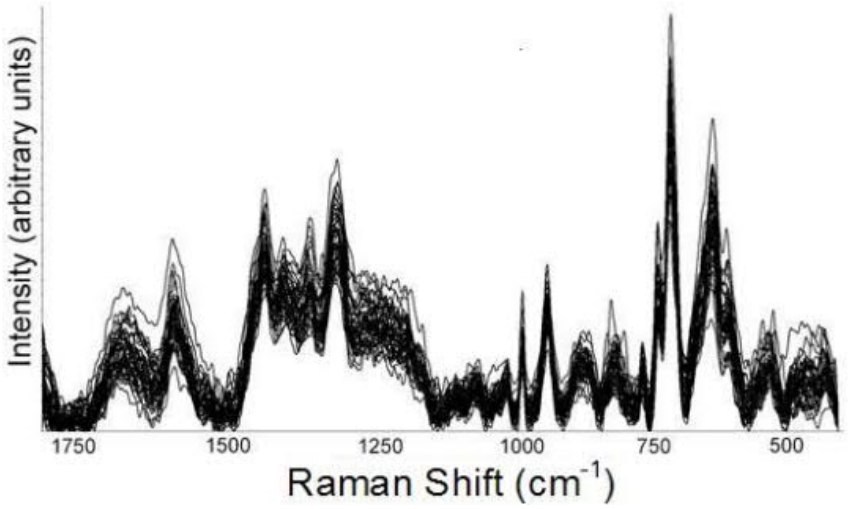

Fig. S21. Linear baseline corrected SERS spectra of 1:5 *E. coli* – *S. enterica* mixture. 400 cm^{-1} ~1800 cm^{-1} range; n = 45.

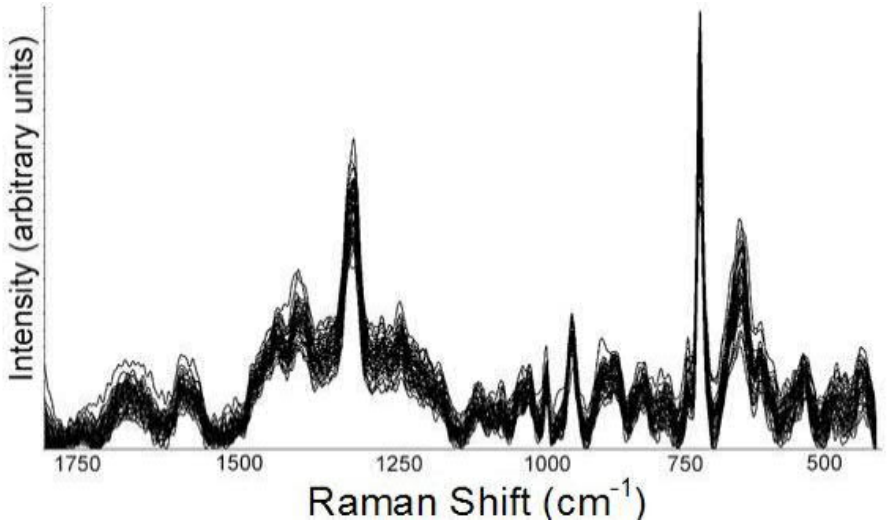

Fig. S22. Linear baseline corrected SERS spectra of 1:2 *E. coli* – *S. xylosus* mixture. 400 cm^{-1} ~1800 cm^{-1} range; n = 45.

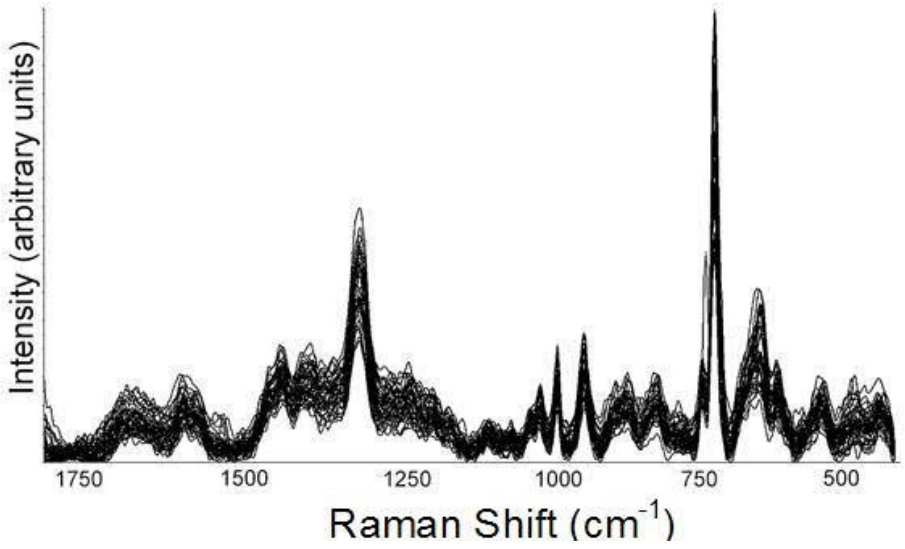

Fig. S23. Linear baseline corrected SERS spectra of 1:5 *E. coli* – *S. xylosus* mixture. 400 cm^{-1} ~1800 cm^{-1} range; n = 45.

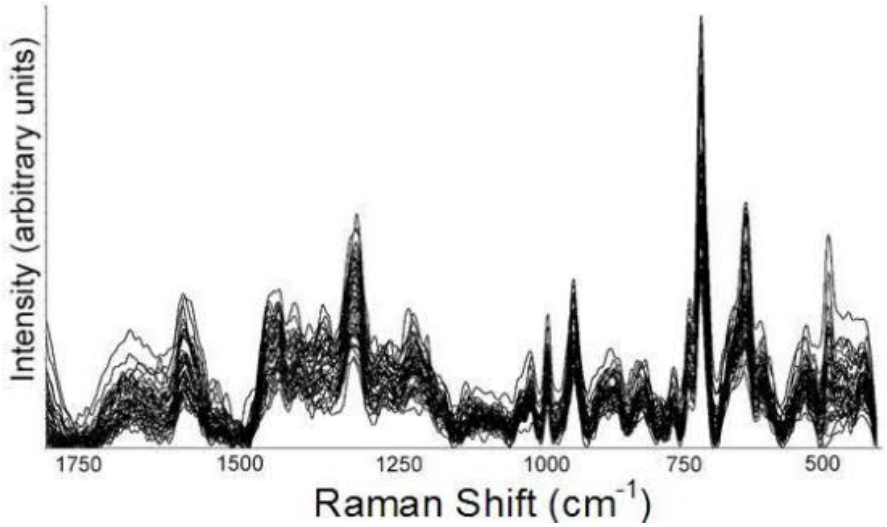

Fig. S24. Linear baseline corrected SERS spectra of 1:2 *S. enterica* – *S. xylosus* mixture. 400 cm^{-1} ~1800 cm^{-1} range; n = 45.

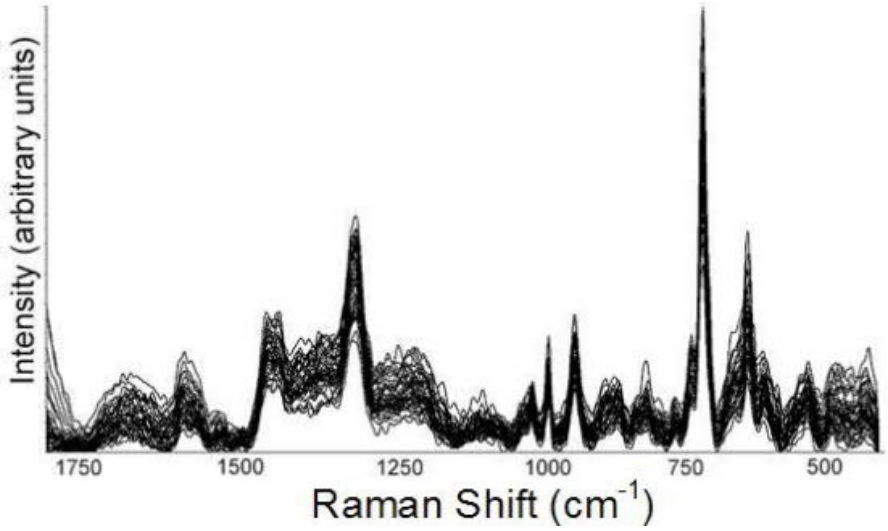

Fig. S25. Linear baseline corrected SERS spectra of 1:5 *S. enterica* – *S. xylosus* mixture. 400 cm^{-1} ~1800 cm^{-1} range; n = 45.

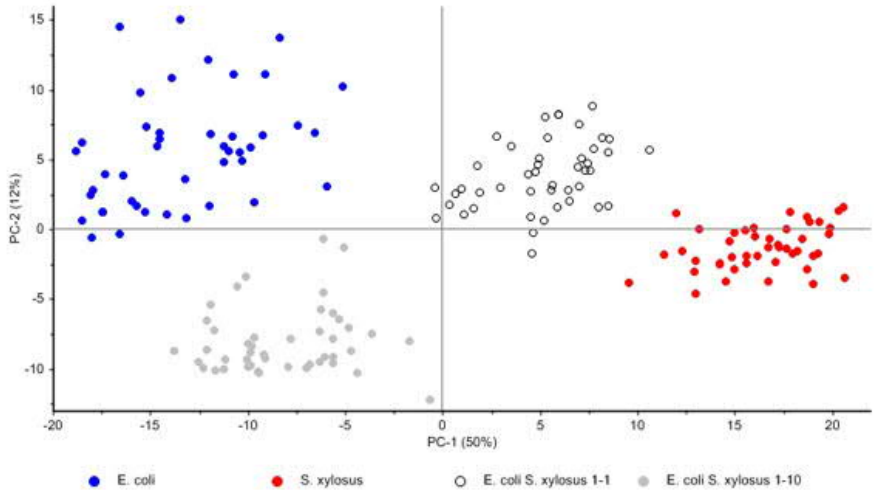

Fig. S26. A: PCA for *E. coli* – *S. xylosus* 10:1 mixtures plotted according to the first two PCs. Blue circle = *E. coli*, red circle = *S. xylosus*, black empty circle = 1:1 mixture, black filled circle = 10:1 mixture (n = 45 for each sample type).

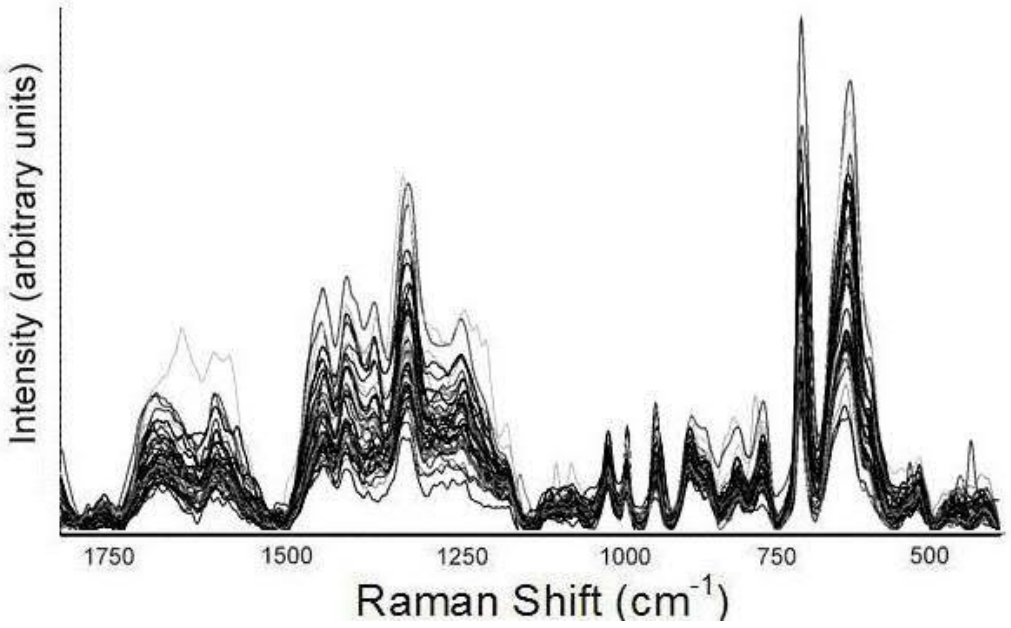

Fig. S27. Linear baseline corrected SERS spectra of 10:1 *E. coli* – *S. xylosus* mixture. 400 cm^{-1} ~1800 cm^{-1} range; n = 45.

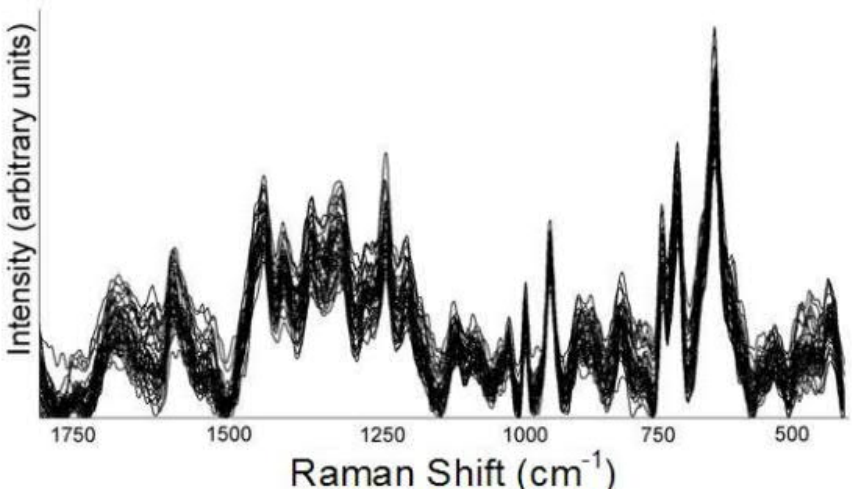

Fig. S28. Linear baseline corrected SERS spectra of *E. coli* suspended in Fanta. 400 cm^{-1}~1800 cm^{-1} range; n = 45.

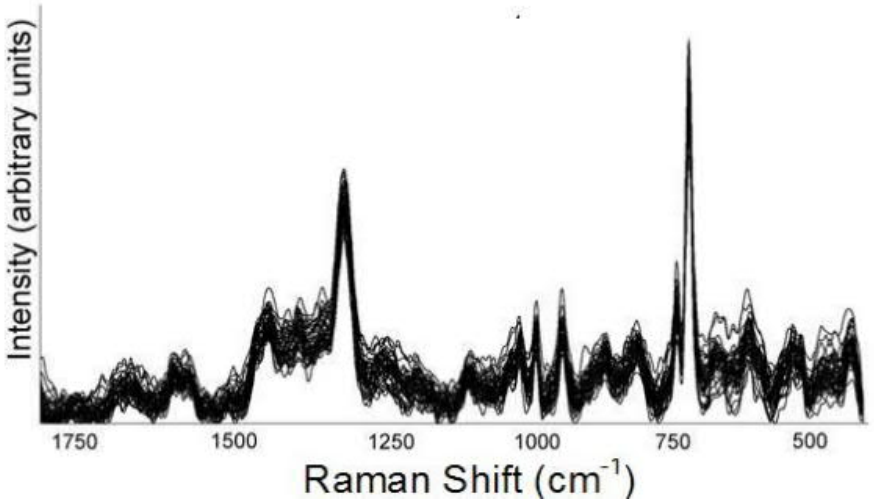

Fig. S29. Linear baseline corrected SERS spectra of *S. xylosus* suspended in Fanta. 400 cm^{-1}~1800 cm^{-1} range; n = 45.

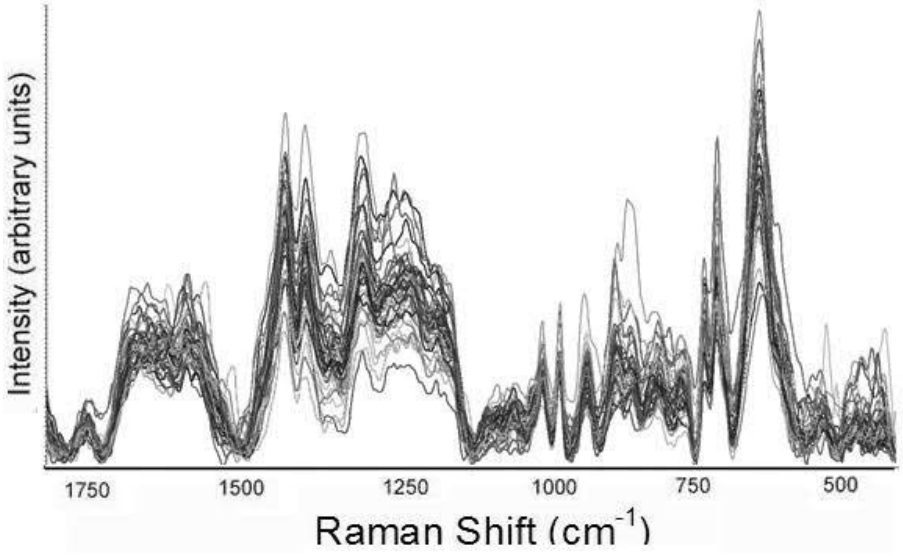

Fig. S30. Linear baseline corrected SERS spectra of *E-coli* grown in Fanta to LB nutrient (1:10). 400 cm^{-1}~1800 cm^{-1} range; n = 45.

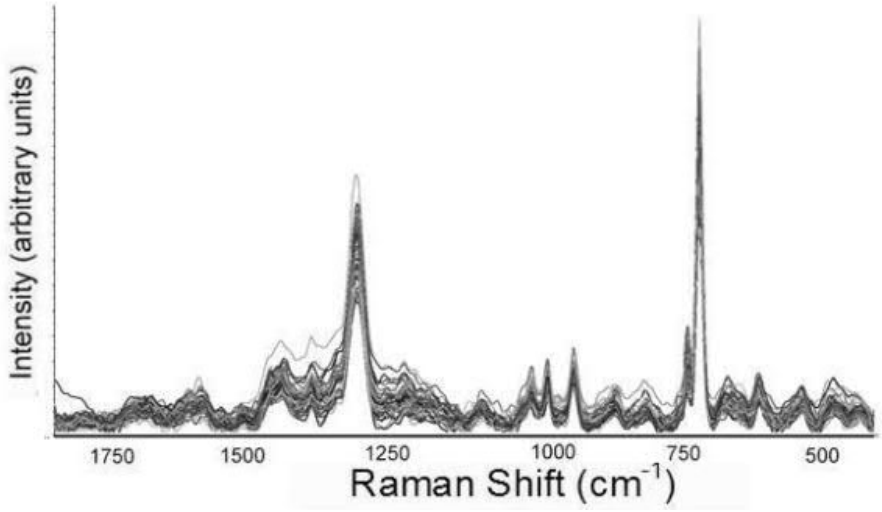

Fig. S31. Linear baseline corrected SERS spectra of *S. xylosus* grown in Fanta to LB nutrient (1:10). 400 cm^{-1}~1800 cm^{-1} range; n = 45.

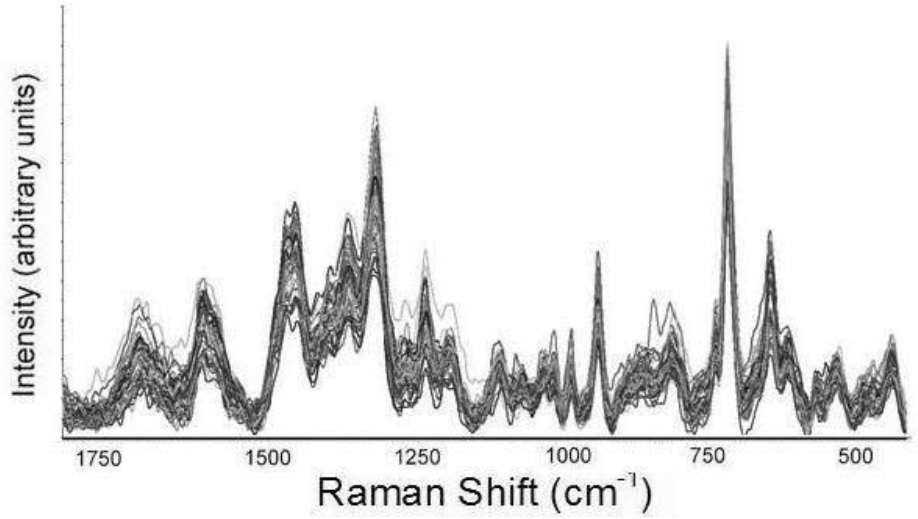

Fig. S32. Linear baseline corrected SERS spectra of 1:1 *E. coli – S. xylosus* mixture suspended in Fanta. 400 cm^{-1} ~1800 cm^{-1} range; n = 45.

Tab S1. List of dominant band assignments and description of relevant biochemical components of the SERS spectrum of *Salmonella enterica*

Wavenumber(cm^{-1})	Assignment [3-8]	Biochemical components of *S. enterica* bacteria
653 vs	ring breathing	guanine base
727 s	ring breathing	adenine of nucleic acids
749 m	ring breathing	thymine of nucleic acids
891 m	C-O sym stretch, C-O-H sym deform and C-O-C sym deform	lipid layer of cell wall and membrane
990~1152 vw	P=O sym stretch	nucleic aicds, phospholipids
1159~1288 m	C-N sym stretch, N-H sym deform C=O sym stretch, Amide III	protein
1327 m	ring stretch	cytosine and uracil of nucleic acids
1411 m	C=O sym stretch	peptidoglycan and disaccharide-pentapeptide of cell wall lipopolysaccharide of outer membrane
1454 m	C-H deform	lipid, carbohydrate and protein
1690 w	C=O stretch, amide I (α-helical structure)	protein

vs-very strong, s-strong, m-medium, w-weak, vw-very weak, sym stretch-symmetric stretch, deform-deformation

Tab S2. List of dominant band assignments and description of relevant biochemical components of the SERS spectrum of *Escherichia coli*

Wavenumber(cm^{-1})	Assignment [3-8]	Biochemical components of *E. coli* bacteria
658 vs	ring breathing	guanine base
730 m	ring breathing	adenine of nucleic acids
751 m	ring breathing	thymine of nucleic acids
897 m	C-O sym stretch, C-O-H sym deform and C-O-C sym deform	lipid layer of cell wall and membrane
1155-1298 m	C-N sym stretch, N-H sym deform C=O sym stretch, Amide III	protein
1331 m	ring stretch	cytosine and uracil of nucleic acids
1416 m	C=O sym stretch	peptidoglycan and disaccharide-pentapeptide of cell wall lipopolysaccharide of outer membrane
1444 m	C-H deform	lipid, carbohydrate and protein
1664 w	C=O stretch, amide I (α-helical structure)	protein

Tab S3. List of dominant band assignments and description of relevant biochemical components of the SERS spectrum of *Staphylococcus xylosus*

Wavenumber(cm^{-1})	Assignment [3-8]	Biochemical components of *S. xylosus* bacteria
666 vw	ring breathing	guanine base
730 s	ring breathing	adenine of nucleic acids
850-940 m	C-O sym stretch, C-O-H sym deform and C-O-C sym deform	lipid layer of cell wall and membrane
1241-1307 m	C-N sym stretch, N-H sym deform C=O sym stretch, Amide III	protein
1327 s	ring stretch	cytosine and uracil of nucleic acids
1449 m	C-H deform	lipid, carbohydrate and protein
1678 vw	C=O stretch, amide I (α-helical structure)	protein

References:

1. B. Nikoobakht, M. A. El-Sayed, Preparation and Growth Mechanism of Gold Nanorods (NRs) using Seed-Mediated Growth Method. Chem. Mater. 15 (2003) 1957-1962.
2. D. Aherne, D. M. Ledwith, M. Gara, J. M. Kelly, Optical Properties and Growth Aspects of Silver Nanoprisms Produced by a Highly Reproducible and Rapid Synthesis at Room Temperature. Adv. Funct. Mater. 18 (2008) 2005-2016.
3. A.C .Williams, H. G. M. Edwards, Fourier Transform Raman Spectroscopy of Bacterial Cell Walls. J. Raman. Spectrosc. 25 (1994) 673-677.
5. W. R. Premasiri, D. T. Moir, M. S. Klempner, N. Krieger, G. Jone II, L. D. Ziegler, Characterization of the Surface Enhanced Raman Scattering (SERS) of Bacteria. J. Phys. Chem. B. 109 (2005) 312-320.
6. K. Maquelin, L. P. Choo-Smith, T. Van vreeswijk, H. P. Endz, B. Smith, R. Bennett, H. A. Bruining, G. J. Puppels, Raman Spectroscopic Method for Identification of Clinically Relevant Microorganisms Growing on Solid Culture Medium. Anal. Chem. 72 (2000) 12-19.
7. K. Maquelin, C. Kirschner, L. P. Choo-Smith, N. Van den Braak, H. P. Endtz, D. Naumann, G. J. Puppels, Identification of Medically Relevant Microorganisms by Vibrational Spectroscopy. J. Microbiol Meth. 51 (2002) 255-271.
8. B. Schrader, ed. 1995, Infrared and Raman Spectroscopy: Methods and Applications. VCH Publishers: NY.